Journal Pre-proof

Ag_2WO_4 as a multifunctional material: fundamentals and progress of an extraordinarily versatile semiconductor

A.F. Gouveia, R.A. Roca, N.G. Macedo, L.S. Cavalcante, E. Longo, M.A. San-Miguel, A. Altomare, G.S. da Silva, J. Andrés

PII: S2238-7854(22)01712-4

DOI: https://doi.org/10.1016/j.jmrt.2022.11.011

Reference: JMRTEC 5909

To appear in: *Journal of Materials Research and Technology*

Received Date: 26 July 2022

Revised Date: 24 October 2022

Accepted Date: 2 November 2022

Please cite this article as: Gouveia AF, Roca RA, Macedo NG, Cavalcante LS, Longo E, San-Miguel MA, Altomare A, da Silva GS, Andrés J, Ag_2WO_4 as a multifunctional material: fundamentals and progress of an extraordinarily versatile semiconductor, *Journal of Materials Research and Technology*, https://doi.org/10.1016/j.jmrt.2022.11.011.

This is a PDF file of an article that has undergone enhancements after acceptance, such as the addition of a cover page and metadata, and formatting for readability, but it is not yet the definitive version of record. This version will undergo additional copyediting, typesetting and review before it is published in its final form, but we are providing this version to give early visibility of the article. Please note that, during the production process, errors may be discovered which could affect the content, and all legal disclaimers that apply to the journal pertain.

© 2022 The Author(s). Published by Elsevier B.V.

Journal Pre-proof

Ag_2WO_4 as a multifunctional material: fundamentals and progress of an extraordinarily versatile semiconductor

A.F. Gouveia[1,2*], R.A. Roca[3,4], N.G. Macedo[2], L.S. Cavalcante[5], E. Longo[3], M.A. San-Miguel[2], A. Altomare[6], G.S. da Silva[4], J. Andrés[1*]

[1]Department of Analytical and Physical Chemistry, University Jaume I (UJI), Castelló 12071, Spain
[2]Institute of Chemistry, State University of Campinas, 13083-970, Campinas, São Paulo, Brazil
[3]CDMF, Universidade Federal de São Carlos, 14800-060 São Carlos, SP, Brazil
[4]Department of Chemistry, Instituto Federal de Educação, Ciência e Tecnologia de Maranha - IFMA, Campus: Monte Castelo. São Luiz, MA, Brazil
[5]PPGQ-GERATEC-CETEM, Universidade Estadual do Piauí, Rua: João Cabral, N. 2231, P.O. Box 381, 64002-150 Teresina, PI, Brazil
[6]Institute of Crystallography-CNR, Via G. Amendola 122/o, 70126 Bari, Italy

Abstract

Silver tungstate (Ag_2WO_4) based materials are intensively studied because of their unique chemical and physical properties. Ag_2WO_4 polymorphs present discrete and intrinsically complex architectures due to a multifaceted framework derived from the different local coordination of Ag and W cations. This review starts with an overview of the synthesis of the three existing polymorphs (α, β, and γ) and their structures. Then, the synthesis methods, surface modification, doping process, formation of solid solutions and heterojunctions, involving Ag_2WO_4, and the effect of electron beam/femtosecond laser irradiation have been exemplified and discussed in detail. Finally, existing challenges and future development are also provided to shed light on the application of highly efficient Ag_2WO_4-based materials

***Keywords*:** α-, β-, γ-Ag_2WO_4 crystals; Semiconductor; Multifunctional material; morphology, Technological applications.

*Email address: amandafernandes.gouveia@gmail.com (A. F. Gouveia) and andres@qfa.uji.es (J. Andrés)
Preprint revised to ***Journal of Materials Research and Technology*** *October 24th, 2022*

1. Introduction

A major challenge for 21st-century scientists is to find novel strategies, concepts, and materials and to guarantee continued and steady technological progress in the following decades. Semiconductor materials, based on metal oxides, have become ubiquitous in scientific research due to their potential to overcome the challenges of availability, high-cost processing, and toxicity, which have been insurmountable to be applied in new technologies. These benefits justify that the US government and EU are investing US$52 and US$48 billion, respectively, in technological development [1, 2]. The family of metallic tungstates is a particularly appealing hunting ground, and a representative member is the silver tungstate (Ag_2WO_4), which offers great structural variability and, consequently, broad technical applicability.

The multifunctional properties of Ag_2WO_4-based materials have been intensively studied, such as high adsorption capacity for cationic dye removal, antibacterial, photoluminescent, antifungal, antiviral, electrochemical sensing, violet-visible photocatalytic performance, lubrication, light-emitting diodes, gate dielectrics, ozone-ethanol-acetone-ammonia gas sensors, electro-catalyst, and so on [3-43]. Moreover, interesting biological properties have been demonstrated for α-Ag_2WO_4, and it has been used as an antimicrobial and anticancer agent [8, 19, 24, 44-47]. Therefore, it is very important to give a complete overview of this oxide material based on its various electronic properties and applications reported in the literature.

The review is subdivided as follows: we begin with the progress made in the different synthesis methods of Ag_2WO_4 polymorphs, and then we continue studying their

structures and morphologies. Subsequently, the solid solutions, doping, and composites are outlined. Afterward, the effect and practical applications of Ag_2WO_4-based materials, induced by an electron beam (EB) and femtosecond (fs) laser irradiation, are summarized, and several applications that are (or can be) positively affected by the development and use of the materials formed by these interactions are discussed. We conclude by suggesting directions for future work to progress in the materials science field. We believe that this review of the above knowledge will help give us a proper perspective to assess the scientific merit regarding the reliability of Ag_2WO_4 as a multifunctional semiconductor for new discoveries and practical applications in the future.

2. Structures for Ag_2WO_4 polymorphs

From a structural point of view, Ag_2WO_4 polymorphs have a complicated network structure with remarkable crystallographic inhomogeneity and intrinsic anisotropy associated with their building blocks, i.e., constituent [AgO_x] and [WO_y] clusters. These clusters present distinct bonding environments of the statistically disordered Ag^+ and W^{6+} cations coordinated with O^{2-} anions. The W^{6+} cation shows three [WO_y] (y = 4, 5, and 6) clusters, while the Ag^+ cation can display different [AgO_x] clusters with low and high coordination numbers, [AgO_x] (x = 2, 4, 5, 6, and 7) (see **Fig. 1(a-c)**). The piling up of these clusters builds the three-dimensional structures.

Ag_2WO_4 crystals exhibit polymorphism, forming either the α-, β- and γ-Ag_2WO_4 [48]: the thermodynamically stable α-polymorph, with orthorhombic structure and space group ($Pn2n$) and point-group symmetry (C_{2v}^{10}); the metastable β-polymorph, with a hexagonal structure and space group ($P6_3/m$) and point-group symmetry (C_{6h}^{2}); and also metastable, the cubic γ-polymorph with space group ($Fd\bar{3}m$) and point-group symmetry (O_h^7) [14, 23, 26, 48-50].

<Insert Fig. 1(a–c)>

The γ-Ag_2WO_4 structure is a well-ordered crystal composed of two clusters, [AgO_6] and [WO_4]. When this symmetry is perturbed, the electron density between both types of clusters is modified, generating a change from the distorted octahedral [AgO_6] and tetrahedral [WO_4] clusters into distorted bipyramid [AgO_5] and trigonal bipyramid [WO_5] clusters, respectively, to render the hexagonal β-Ag_2WO_4 polymorph. These structural rearrangements involving the clusters reach the maximum crystalline adaptation when the hexagonal structure becomes orthorhombic, giving rise to the α-Ag_2WO_4 structure. In this structure, three different tetrahedral [WO_4] clusters appear, while two different deltahedral [AgO_7] clusters, one distorted octahedral [AgO_6] cluster, two distorted tetrahedral [AgO_4] clusters, and one angular [AgO_2] cluster is present. Therefore, the local coordination of the metal cation in the bulk corresponds to the specific number of surrounding oxygen anions. However, these clusters present undercoordination at the surfaces, i.e., a minor number of oxygen anions around Ag, which is responsible for most of the semiconductor properties.

From an electronic point of view, these clusters, in turn, display low or high electron density, rending different band gap values for each exposed surface. When

performing an experimental measurement of the band gap, an average value over all exposed surfaces at the morphology is obtained. On the other hand, the electron transfer process depends directly on the electron distribution at each surface and the electronic structure of the undercoordinated/distorted clusters at the surface. Therefore, the semiconductor can be considered a dynamic system in which the clusters are quantum clusters to carry out the absorption/emission of an electron in the ground and excited state, respectively. The different types of clusters on the same surface may have different properties and functions depending on the number and nature of defects. In the Ag_2WO_4 semiconductor, the top of the valence band (VB) is composed mainly of hybridized Ag 4*d* and O 2*p* orbitals, which can lift the top position of the VB and narrow down the band gap. The bottom of the conduction band (CB) consisting of delocalized *s* and/or *p* orbitals displays significant dispersity so that it possesses a high migration efficiency of photogenerated electrons [51, 52]. The electronic properties and applications can be associated with the nature and rearrangement of the Ag−O and W−O chemical bonds, which range from ionic, covalent, to metallic, as well as unique electronic properties [53]. Recently, Moura et al. have presented a temperature-dependent Raman study on the structural changes induced by the temperature in the β-Ag_2WO_4 crystal. In these transitions, the changes that occurred in the Raman spectra were characterized by the appearance and disappearance of new Raman modes. The results lead to a complex sequence of phase transitions involving β-hexagonal to α-orthorhombic, α-orthorhombic to hexagonal, and β-hexagonal to α-orthorhombic again [54].

It is well known that many properties of solid materials, including semiconductors, are controlled not only by their geometry and electronic structure but also by the nature and defects in their crystal structure [55-58]. In this sense, it is essential to understand the influence of defects on the activity and performance for further optimization of the semiconductor system. In transition metal oxides, defects can be associated with anionic vacancies (oxygen vacancies) and cationic vacancies (metal vacancies or complexes vacancies). These vacancies act not only as electron-hole recombination centers by capturing a free electron and hole but also break the electronic structure of an otherwise perfectly periodic crystal. Our group is engaged in a research project devoted to understanding the nature of the defects in semiconductors. Positron annihilation lifetime spectroscopy measurements in conjunction with first-principles calculations, at the density functional theory level, X-ray diffraction (XRD), Raman spectroscopy, photoluminescence emissions, and field emission gun scanning electron microscopy techniques render that main defects are composed by Ag vacancies and that the concentration of this type of defect increases with the irradiation time [59].

Journal Pre-proof

3. Synthesis of the different polymorphs of Ag_2WO_4-based materials

One of the most sought-after goals in materials science is the acquisition of knowledge and the complete understanding of the different phases of a given material, which is essential to identifying which polymorph is best suited for a specific technological application. Changes in the concentration and preparation of the reactants, the nature of the

solvents, and/or external conditions (such as pressure and temperature) have been traditionally employed to control the synthesis of the different polymorphs. Therefore, this section provides a brief analysis and survey of the literature about Ag_2WO_4 preparation.

Since it was first reported in the literature in 1949 by Rabes and Schenck [60], through classical experiments, metallic silver (Ag^0) is oxidized to silver ion (Ag^+) at high temperatures and reacts with tungsten oxide (WO_3) to form Ag_2WO_4 and another type of tungsten oxide (W_3O_8) following the chemical reaction: $2Ag + 4WO_3 \rightarrow Ag_2WO_4 + W_3O_8$.

Fig. 2(a-c) displays the main steps employed in the initial and traditional synthesis method related to solid-state reaction or oxides powder mixtures to obtain Ag_2WO_4.

<Insert Fig. 2(a–c)>

As can be observed in **Fig. 2(a)**, the initial stage corresponds to traditional solid-state reactions of oxides powder mixtures, 1 mol of silver (I) oxide (Ag_2O) and 1 mol of tungsten (VI) oxide (WO_3), with black and canary yellow color, respectively. In the second stage, after the homogeneous mixing of the two oxides, both are placed in a rotating mill with balls of ZrO_2:Y with high hardness for better homogenization of this mixture; ethyl alcohol is employed to facilitate the interaction between the contact surface of the Ag_2O and WO_3 powders for several grinding cycles for 4 to 6 hours and then placed in an oven for dry power [61], as shown in **Fig. 2(b)**. Finally, this more homogeneous and drier mixture was heated in a muffle furnace between 350 and 950 ºC for 2-24 h to obtain α-Ag_2WO_4 purple color powder by means of solid-state reaction: $1Ag_2O$ and $1WO_3 \rightarrow$ α-Ag_2WO_4, as displayed in **Fig. 2(c)**.

Later, some papers reported on thermochemistry and conductivity studies on this material. In 1973, Takahashi *et al.* [62] reported the study of a novel high ionic conductivity solid electrolyte, AgI-Ag_2WO_4, at ambient temperature. Two years later, Skarstad and Geller [49] determined data exclusively by XRD patterns, associated with the orthorhombic structure of the α-Ag_2WO_4 phase. Bottlebergs et al. [63] studied the phase diagram and ionic conductivity of the Na_2WO_4-Ag_2WO_4 system. Additionally, several groups examined the thermal capacity, kinetics, and solid-state reaction mechanisms of Ag_2WO_4 with bromide and mercury chloride [64-66]. In addition, α-Ag_2WO_4 has been prepared as a "composite thin film" (polyvinyl chloride-C-Ag_2WO_4) and used as an electrode (cathode) for possible application in solid-state lithium batteries. Also, α-Ag_2WO_4 was prepared as a composite coating to be used as a high-temperature solid lubricating material for wear applications [28, 67]. The synthesis of β-Ag_2WO_4 was first reported by Mckechnie et al. in 1979 [68]. Schiraldi and Pezzati observed the application of Ag_2WO_4 crystals as super-ionic conducting glasses in 1981 [69]. The following year, van den Berg and Juffermans [48] discovered the presence of polymorphism for Ag_2WO_4 crystals: the metastable phases beta (β-Ag_2WO_4) related to the hexagonal structure and the gamma (γ-Ag_2WO_4) with a cubic structure.

The Ag_2WO_4 crystals were prepared by different methods, such as solid-state reactions, oxide mixtures, mechanochemical [14, 70, 71], precipitation with calcination at elevated temperatures [72], and crystal growth utilizing a Czochralski process [73]. However, these preparation methods require high temperatures, long processing times, and sophisticated equipment with high maintenance costs. In recent years, improved synthesis

methods have been developed to overcome some problems of the older approaches to obtain crystals with different sizes, shapes, and single phases. The most frequently employed synthesis is controlled precipitation [74-76] *via* a simple ion-exchange method at room temperature [77], conventional hydrothermal (CH) [10, 78-80], and microwave-assisted hydrothermal (MAH) [81].

In particular, the CH method has been used recently in the preparation of different tungstates with different sizes and shapes [82-84]. Therefore, this method has received much attention from the scientific community due to its numerous advantages over other methods, such as the use of an environmentally friendly solvent (water) and a low processing temperature (≈ 200 ºC) [85]. By using the CH method, crystalline materials are obtained involving the dissolution of aqueous soluble reagents or precursors with or without the presence of a mineralizer (chemical bases) under temperature and pressure [86]. Generally, the materials obtained by this method are very fine, crystalline, and easily dispersed [87]. Recently, this method has been presented in the literature [10, 78] to prepare nanorods and nanofibers of Ag_2WO_4. However, obtaining Ag_2WO_4 nanocrystals by this method requires long processing times (12-24 h) due to the low reaction kinetics [10].

The use of microwave energy in CH systems allows the development of a new synthesis method with enhanced processing capabilities for accelerating the reaction rate and promoting crystallization due to the increase in the number of effective shocks and the high heating rates [88]. In typical MAH processing, the “chemical reaction acceleration” factor is favored by the high frequency of electromagnetic radiation (2.45 GHz) that interacts with the permanent dipoles of the liquid phase (water) [89]. The movement of the

permanent or induced dipoles in the dispersed phase results in the rapid heating of the particles and consequently favors an increase in the reaction temperature. By this mechanism, coupling occurs between the reagents involved in the chemical reaction, which results in the formation of the products [90, 91]. Furthermore, processing in a MAH system may offer other advantages, such as different forms, highly pure phases, shorter processing time, and low energy consumption [92].

More recent research has performed methods of synthesis and stabilization of such metastable phases. Wang et al. [26] obtained superfine β-Ag_2WO_4 antibacterial powders by supersonic-assisted homogeneous precipitation from a chemical reaction between $AgNO_3$ and sodium tungstate dihydrate (Na_2WO_4•$2H_2O$). Another example is the fabrication of hierarchically porous metastable hollow nanospheres of β-Ag_2WO_4 by Wang et al. [93]. They employed the polymer poly(methyl methacrylate) (PMMA) as a template and inhibitor of the transformation to the α-Ag_2WO_4. PMMA added to the $AgNO_3$ solution before the addition of Na_2WO_4**.**$2H_2O$ solution acted as a template by arranging into cross-linked micelles with an inner hydrophobic backbone and outer hydrophilic carboxylic acid groups (–COOH). A core-shell structure was formed composed of inorganic Ag_2WO_4 nanoparticles (NP) in the shell and a PMAA at the core. The PMAA core could be easily removed by washing with water and alcohol, forming Ag_2WO_4 hollow nanospheres. The obtained product was composed of hollow nanospheres (200-500 nm in size with a wall thickness of approximately 20 nm) consisting of an assembly of many small NPs with a diameter of less than 10 nm.

Sonochemical (SC) synthesis was used by Zinatloo-Ajabshir et al. [94] to obtain α-Ag_2WO_4 nanostructures as visible-light-driven photocatalysts for wastewater treatment. The authors reported that the sample synthesized using sodium o-dodecylbenzenesulfonate as a surfactant improved the photocatalytic activity of the material. The α-Ag_2WO_4 rod-like microcrystals were obtained by Nobre et al. [47] using sonochemistry and sonochemistry followed by CH methods in which the antimicrobial properties of the samples were investigated. Recently, the sonochemical method was employed to achieve the control size and morphology of the α-Ag_2WO_4 materials by using three carboxylic acids (tartaric, benzoic, and citric). The degradation process of Rhodamine B (RhB) dye was excellent, reaching 100% degradation in 60 minutes for the as-synthetized samples with citric acid, which have nanoscale dimensions [95].

In 2014, our research group performed two different synthesis methods that led to the formation of two Ag_2WO_4 phases. One was a coprecipitation (CP) reaction followed by a MAH method that resulted in microsized irregular polyhedral crystals of the α-Ag_2WO_4 phase, and the other was a simple CP at 70 °C and pH 4, which resulted in nanowires and polyhedral crystals of the β- and α-Ag_2WO_4, respectively [9]. Another synthesis of nanorods was performed by the CP method followed by an SC treatment [13]. In 2014 and 2016, our research group employed a MAH treatment after a CP reaction in the presence of polyvinylpyrrolidone (PVP) surfactant, obtaining nanorods with gas sensor applications [6, 7]. Recently, Rakshitha et al. used the CP method to obtain the Ag_2WO_4 with nanoflower-like morphology and enhanced photocatalytic activity [41].

Our research group synthesized multifaceted rod-like microcrystals of β-Ag_2WO_4 by a simple CP reaction at room temperature, which was further analyzed by field emission scanning electron microscopy (FE-SEM) and transmission electron microscopy (TEM) to observe the *in-situ* growth of Ag-NPs on the surface of the material [31]. The same synthesis method was further employed and combined experimental and theoretical studies were performed by Lemos et al. [96] and Roca et al. [31] to investigate the β-Ag_2WO_4 metastable polymorph.

Chen and Xu [5] synthesized α- and β-Ag_2WO_4 phases by the same method (CP reaction with the dropwise addition of $AgNO_3$) but at different concentrations. The first was the addition of 50 mL of 0.40 M $AgNO_3$ to 50 mL of 0.20 M Na_2WO_4, which resulted in the α-Ag_2WO_4. The second method was similar, but in this case, 100 mL of 20 mM $AgNO_3$ was added to 1 L of 1.0 mM Na_2WO_4 related to the β-Ag_2WO_4. Both phases have a rod-like morphology, but the β-Ag_2WO_4 crystals were larger (the average grain size of α-Ag_2WO_4 was 1.78×0.56 μm, and that of β-Ag_2WO_4 was 3.10×0.79 μm). Our group successfully used the dropwise precipitation method to synthesize the β-Ag_2WO_4 microcrystals using aqueous media at a low temperature (15 °C). The strategy of synthesis was: 4 mmol of $AgNO_3$ in 50 mL of water was cooled to 15 °C and added dropwise at 2 mL min^{-1} to a solution of 2 mmol of Na_2WO_4**.**$2H_2O$ dissolved in 50 mL of deionized water at 15 °C [96]. This practical and controllable synthesis method may inspire the synthesis of metastable phases of other complex metal oxides.

In 2015, Ramezani et al. [97] employed the electrochemical deposition method to prepare β-Ag_2WO_4 in different morphologies at the nanoscale by simply varying the

parameters of the conditions, such as the concentration of the Na_2WO_4 electrolyte solution, voltage, stirring rate, and reaction temperature. As a result, they obtained nanosheets, nanorods, flower-like structures, and agglomerates of those morphology types. Other synthetic strategies, based on the use of Ag_2WO_4 composites [98] and dopants [99] to stabilize the β-Ag_2WO_4 metastable have been reported.

Liu et al. [100] conducted a study by the CP synthesis at pH values varying from 1.5 to 6.8 and W concentrations to obtain Ag_2WO_4 nanowires. For the Ag_2WO_4 nanofibers, the diffraction peaks at 27.5° and 41.6° belong to the (121) and (132) facets of β-Ag_2WO_4, while the other peaks are all attributable to α-Ag_2WO_4 crystals, suggesting that the Ag_2WO_4 sample is mainly the α-Ag_2WO_4 phase and contains a small amount of the β-Ag_2WO_4.

Our research group performed a comparative study among SC, CP, and CH methods. The results were similar, and eight-faceted rod-like microcrystals were obtained [11]. Our research group also attained these microcrystals in 2013 in a rapid stoichiometric CP reaction at 90 °C without external agents and *via* MAH in 2014 and another study with PVP surfactant, but this time, the morphologies were accompanied by other shapes, such as cubic and triangular crystals [12,17,19]. In our recent article, we report the selective synthesis of each α-, β-, γ-Ag_2WO_4 polymorphs through a simple precipitation route at ambient temperature by controlling the volumetric ratios of the $AgNO_3/Na_2WO_4{\bullet}2H_2O$ precursors in solution [101]. This selective synthesis allows us to control the formation of the desired polymorph. A schematic representation of the different synthetic procedures for Ag_2WO_4 polymorphs is presented in **Fig. 3.**

<Insert Fig. 3>

4. Morphology of Ag_2WO_4 polymorphs

The first article providing information about the microscopic aspects of α-Ag_2WO_4 was published by Yu et al. [78] in 2003, in which a facile and general low-temperature solution approach was employed to synthesize a family of single-crystalline tungstate nanorods and nanowires, such as $ZnWO_4$, $FeWO_4$, $MnWO_4$, Bi_2WO_6, Ag_2WO_4, and $Ag_2W_2O_7$. Their proposal was based on a hydrothermal crystallization method of an aqueous dispersion containing amorphous particles of each oxide, obtained by direct precipitation at room temperature.

Most studies related to α-Ag_2WO_4 crystals report the occurrence of a rod-like shape morphology with nano or micro dimensions. The HM is an appropriate route for the synthesis of fine, crystalline materials [87], while CP reactions in the absence of surfactants, capping agents, or special treatments tend to favor the synthesis of rods with larger dimensions. This was the case for the elongated rods obtained by Sreedev et al., with average diameters of 0.30 μm and lengths of up to 5 μm. They performed a simple CP reaction from equimolecular quantities of Na_2WO_4 and $AgNO_3$ at room temperature and pH=7, followed by calcination treatments between 500 and 600 °C for 3 hours, resulting in the dark to light violet precipitates [102-104]. Although the obtained rods were above the nanoscale, the authors considered the materials nanophase, due to the good aspect ratio.

Some studies observed the effect of pH on the formation of different nanostructures. For example, a deep interpretation is given by the work of Yu et al. [10, 78], in which the influence of pH on the morphology of the as-synthetized samples was analyzed, and Ag_2WO_4 nanorods and $Ag_2W_2O_7$ nanowires (approximately 50 nm of diameter and length up to micrometers) at pH=9 and 2 were obtained, respectively. The authors suggest that the growth process of nanoparticles occurs through a typical hydrothermal ripening process, with the direct mixing of two solutions leading to a larger number of amorphous particles. The larger particles grow at the cost of the smaller ones, with the adjustment of pH significantly affecting the composition of other species. Summarily, the authors cite references [105] and Gibbs-Thomson's theory to establish a relation between the chemical potential of crystals and the one-dimension growth.

Zhang et al. [15] obtained rods with sizes from 200 to 600 nm, with a diameter range of 60-100 nm, and some plate-like particles, verifying the key role of basic pH. They also argue that the formation of the rods occurs through the formation of tiny crystalline nuclei that takes place first, followed by the growth of larger particles and posterior aggregation of some rods, explaining why the plate-like particles are also observed [78, 106].

In 2005, George et al. [75] synthesized α-Ag_2WO_4 fibers of 0.5μm in a diameter and approximately 100 μm in length, while the rods present diameter of about 30 nm. They used diluted reactant and precursor concentrations between 0.003-0.001 M for silver nitrate and 0.0015-0.0005 M for sodium tungstate and with a slightly basic pH, staying in suspension overnight. According to the authors, below this concentration, the fiber growth

is not visible, while above, the fiber growth is inhibited by the precipitation of Ag_2WO_4, which hinders long fiber growth.

Ng and Fan reported the synthesis of highly uniform one-dimensional (1D) α-Ag_2WO_4 nanostructures with controllable aspect ratio, and they also investigated the growth mechanism of this material. According to the authors, the aspect ratio of the 1D materials is tuned by varying the duration of stirring during the initial synthesis period, and the results of the reaction intermediates bring to light a three-stage growth mechanism involving the directed aggregation of spherical building blocks [107].

Surfactants can be employed to modulate morphology and, consequently, the functionality of a material. Sodium dodecyl sulfate was used in MAH synthesis at different temperatures (100 °C – 160 °C) to tune the morphology of α-Ag_2WO_4 and find a relationship between the photocatalytic/antibacterial activity and morphology. The results show that the lower MAH temperature (100 °C) generated an eight-facet hexagonal rod-like shape elongated along the [010] direction, while within higher microwave temperatures, new facets appear, resulting in crystals with 12 facets (120 °C – 140 °C), and crystals with 14 facets (160 °C). Photocatalytic activity measurements on the RhB dye and Rhodamine 6G (Rh6G) dye degradation show that this 14-facet crystal was the most efficient photocatalyst under UVC-light, which the authors relate to the presence of the higher values of surface energy (E_{surf} = 0.83 J m^{-2}) of the (110) plane. However, the antibacterial activity tests (*Escherichia coli* (*E. coli*) inactivation) indicated that the 8-facet crystal was the most efficient, which they attribute to a different mechanism involving direct interaction between specific (010) and $(0\bar{1}0)$ surfaces and cell surfaces [24]. This

surfactant was used to obtain, for the first time, a morphology very close to a previously calculated cubic-like morphology [108, 109]. The as-synthesized crystals have a cuboid shape formed by the junction of two or more cubes in one direction, resulting in elongated cubes with average sizes of 200 nm [109]. Although the importance of the study for the relation with previous theoretical works, this morphology showed to be more inactive as a photocatalyst when compared to the most obtained eight-facet hexagonal micro-rods. However, in 2019, a sequential study was published showing that this cuboid morphology, when irradiated by an fs laser, provokes the formation of Ag/α-Ag_2WO_4 composite 64 times more efficient against *Methicillin-susceptible Staphylococcus aureus – MRSA*, in comparison to the non-irradiated morphology, and 2 times higher than the rod-like irradiated morphology [110]. Very recently, the toxicity of this morphology and also rod α-Ag_2WO_4 samples were investigated to freshwater microalga *Raphidocelis subcapitata* at the cellular and population levels [111,112]. Both caused population growth inhibition, being the rod morphology 1.7 times more toxic than the cubic.

By using different solvents (water, alcoholic solution, and ammoniacal solution) [8] two morphologies could be observed, micro-rods in the alcoholic solution and flowerlike structures in water and the ammoniacal solution. A considerable number of three-dimensional (3D) flowerlike α-Ag_2WO_4 microcrystals were observed in the aqueous solution. The observed structures were essentially composed of aggregated nanorod particles exhibiting partial orientation and attachment on the irregular facets. The same 3D flowerlike α-Ag_2WO_4 structures are obtained using the ammoniacal solution. However, in this case, the crystals exhibit three surfaces, with the (001), (101), and (010)

crystallographic planes, which are more defined than the crystals obtained using water as solvent. With the synthesis using the alcoholic solution, α-Ag_2WO_4 nanorods with three surfaces were observed, and the same crystallographic planes as those observed in the case of the α-Ag_2WO_4 structures synthesized using the ammoniacal solution.

Dimethyl sulfoxide was employed as a solvent during the synthesis by using the CP method, and the injection of the reactants was carefully controlled. As a result, rectangular rods with the exposed (010), (001), and (100) facets were synthesized with sizes from 0.27 to 0.67 μm in height and 0.07 to 0.15 μm in width [113]. In this work, the effect of an SEM and TEM electron beam interaction was also investigated. It was observed, for the first time, besides the Ag^0, the presence of silver oxides (Ag_2O and Ag_3O_4) on the extruded material.

In 2020, the potential of ethylenediamine complexing agent to modulate the α-Ag_2WO_4 morphology and structural properties was demonstrated, obtaining microflowers with favorable optical properties [114]. Additionally, the morphological evolution and antibacterial (against *Staphylococcus aureus*) and photocatalytic activity for degradation of RhB dye with α-Ag_2WO_4 as catalyst obtained by the CP method followed by microwave irradiation for different times were also analyzed by our research group in 2020 [115]. We found that the local coordination of superficial Ag and W atoms (i.e., incomplete $[AgO_y \cdot zV^x_O]$ and distorted $[WO_6]_d$ and $[AgO_4]_d$ clusters) on each exposed surface of the corresponding morphology dictated the antibacterial and photocatalytic activities of α-Ag_2WO_4.

Although α-Ag_2WO_4 crystals are the most investigated and stable phase of Ag_2WO_4 material, it might exist in more than one structure, as previously mentioned [48, 49, 68]. Subtle differences in pH and the heating of the solution appear to determine which of the polymorphs is obtained, but accurate powder data were not provided for the different forms, and polymorphic behavior was not investigated in detail. The inferior number of studies referring to the metastable phases is due to the difficulties associated with the isolation of phases that are non-thermodynamically favored, such as the β- or γ-phases of Ag_2WO_4, which are also unsuitable for practical applications, given the possibility of the transition to the α phase over time.

The hexagonal Ag_2WO_4 phase with multilevel sphere clusters of 2.5–2.8 μm in diameter composed of several second-level spheres (approximately 0.8 μm in diameter) was synthesized for the first time by Zhang et al. [33] with the help of an eggshell membrane and acrylamide as templates. The authors showed the importance of the acrylamide template using the same synthesis method, with and without the polymer. Thus, in the presence of the polymer, symmetric and concentric sphere clusters were built. In the absence of the polymer, but in the presence of an eggshell membrane, sphere-like structures, but not clusters, were the products. However, only dendritic crystals were formed in the absence of both membrane and polymer. The monomers actuated, not only as an auxiliary template but also as an absorber of photogenerated electrons, forming PAM through a polymerization reaction.

The γ-Ag_2WO_4 crystals with cubic phase were obtained by our research group in 2017 *via* a CP reaction at low temperatures (0-5 °C) [116]. In this study, first-principles

calculations and Wulff construction were performed to display the available morphologies of this polymorph. The experimental morphologies observed by scanning electron microscopy (SEM) were nearly spherical, with small nanocrystals with a cuboid structure on the large microcrystal surfaces, for the 10 min reaction, while the samples corresponding to a 20 min reaction time had the most microparticles with irregular or approximately spherical structures, although some faceted particles were also found. These faceted NPs were observed to be rod-shaped [116]. In addition, this metastable γ-Ag_2WO_4 phase has recently been successfully synthesized and stabilized by the CP method assisted by PVP at room temperature [117]. Particle formation with octahedral morphology and preferential growth in the (111) plane is favored in the presence of this surfactant.

The promissory antimicrobial properties of Ag_2WO_4 microcrystals were studied by Bastos et al. against several pathogenic bacteria stains (gram-positive and gram-positive bacteria). The results showed a minimum inhibitory concentration less than the positive control [80]. Due to the current COVID-19 pandemic, our research group has developed the next generation of innovative materials with enhanced anti-SARS-CoV-2 activity to prevent the spread of this virus within the community. In 2022, we reported the synthesis of chitosan/α-Ag_2WO_4 composites generated by fs laser irradiation. This material is very efficient in eliminating bacteria (*E. coli*, *MRSA*, and the yeast strain *Candida albicans* – *C. albicans*) and SARS-CoV-2 by contact [118].

A fundamental framework, based on the combination of first-principles calculations and advanced electron microscopy techniques, was developed to obtain the available morphologies of different semiconductors [108, 119-126]. The evolution of the

morphology has been interpreted through equilibrium considerations by using the Wulff method [127], in which the increases/decreases of the surface energy values are the driving force to accompany the appearance of a given exposed surface at the morphology. We showed that the predicted theoretical morphology could match the experimental ones, thereby rationalizing the reaction pathway along the synthesis process. This strategy opens the door for the rational design of semiconductors to enhance the performance of a desired technological application. The high degree of coincidence between theory and experiments suggests that this model has a more general scope of application in different metal oxides, as reported by different research groups [128-138].

Fig. 4 illustrates some morphologies that the α-, β-, γ-Ag_2WO_4 polymorphs can exhibit, and the complete map of morphologies can be found in the literature [31, 108, 116].

<Insert Fig. 4>

Based on the detailed analysis of the atomic coordination environment of surface atoms, we can find a relationship between the material properties (photocatalytic and biocide activities) and the exposed surfaces at the morphology. This is an excellent strategy not only to rationalize and explain the behaviors and properties of the materials but also to explain the corresponding action mechanism [139].

Several strategies can be utilized to improve the activity of Ag_2WO_4 polymorphs, such as solid solutions and doping, composites, and EB and fs irradiation (**Fig. 5**). The next sections will address these issues.

<Insert Fig. 5>

5. Solid solutions and doping

The aim of the research is to improve some properties of materials or even create new applications for them. This proposal can be achieved through the modification of the synthetic route, such as using different temperatures, a change of solvent, and adjusting the methodology for obtaining the material. Another way to achieve this goal can be through the addition of different atoms from the precursors to the reaction medium to generate a solid solution or a doping process.

Doping and solid solutions are important and well-demonstrated strategies for maintaining the integrity of the material's crystal structure. At the same time, physicochemical properties are effectively tuned by changing the crystal parameters, morphology, and electronic structure, among others. Therefore, the rich chemistry of Ag_2WO_4 is often modified, intentionally or unintentionally, through the inclusion of defects and dopants. Kumar et al. [99] have proven that the doping process involving Eu^{3+} cations is an interesting strategy for the stabilization of the hexagonal metastable β-Ag_2WO_4 using the CP method at room temperature. In that report, no changes were observed in the α-Ag_2WO_4 crystal structure until 1.0 mol% Eu^{3+} doping, and for 2.0 mol%, the β-Ag_2WO_4 crystals were stabilized, inhibiting the hexagonal-to-orthorhombic phase transition. Optical characterization, time-resolved photoluminescence, and temperature-dependent studies

supported the origin of the spectral findings. For both α- and β-Ag_2WO_4 phases, the peak emission has been attributed to the charge transfer transition within tungsten octahedra and tetrahedra in α- and β-Ag_2WO_4, respectively.

Our early studies showed that the Eu^{3+} cations are doping $Ag_{2-3x-y}Eu_xLi_yWO_4$ (where x = 0.01, y = 0.01, 0.02, and 0.03 mol) [37] and $Ag_{2-3x}Eu_xWO_4$ (with x = 0.01, 0.02, 0.04, and 0.08 mol) [140], and they were efficiently synthesized by the CP method at 90 °C for 30 min. For all samples, the XRD patterns can be indexed to the pure orthorhombic α-Ag_2WO_4 phase, and the FE-SEM analysis revealed nanorod-like microcrystals. The structural refinement data and the emission spectra analysis (lifetime decays) suggest that Eu^{3+} cations occupy at least two crystallographic sites (probably Ag sites on clusters coordinated by seven O atoms, [AgO_7]). In the latest report, Li^+ cation addition facilitated Eu^{3+} cation incorporation and the emission of red light much more efficiently. The *Commission Internationale de l'Eclairage* coordinates [141] confirmed the classification of this material as a potential phosphor in the visible range.

Similar studies have been extended for other rare earth dopant ions. These works describe the structural and luminescence properties of α-$Ag_{1.97}RE_{0.01}WO_4$ for RE = Pr, Sm, Eu, Tb, Dy, and Tm [142] and for RE = Eu, Dy, Tm, and Er [143] synthesized using a simple CP method. The X-ray photoelectron spectroscopy properties of these phosphors were reported for the first time [142] and efficient energy transfer from the WO_4^{2-} group to RE^{3+} cations was observed. Additionally, these systems showed the possibility of color tuning by simple RE dopant selection. These pieces of evidence also contribute to the development of new materials for temperature sensing (by the emission intensity

dependence on temperature) and their use for optical applications, including light-emitting diodes and lasers. The fluorescence property of Eu^{3+} ions in the α- and β-Ag_2WO_4 was investigated by Huangfu et al. The results have shown that the metastable β-Ag_2WO_4 structure is more favorable as a host material for Eu^{3+} than α-Ag_2WO_4, and the β-Ag_2WO_4:Eu presented about 60 times superior fluorescence intensity [144].

The effects of solid solution formation due to the incorporation of transition-metal (TM) cations have been investigated from a combination of experimental and theoretical studies [37, 143, 145-149]. From α-$Ag_{2-2x}TM_xWO_4$, cations such as Ni ($0 \leq x \leq 0.08$) [119], Zn ($0 \leq x \leq 0.25$) [148] and Cu ($0 \leq x \leq 0.12$) [145, 146] were used for substitution of Ag atoms. In the recently published article, Pereira et al. showed that the increase in the Cu^{2+} cations content in the α-$Ag_{2-2x}Cu_xWO_4$ solid solutions provoked a change in the morphology to a nanoplate-like morphology formed only of (010) and (101) surfaces enhancing the antibacterial and antifungal activities against MRSA and *C. albicans*, respectively [150]. In another publication, Marzieh et al. investigated the behavior of $Ag_{1.8}Zn_{0.1}WO_4$ nanoparticles in the production of singlet oxygen, $^1O_2$, and hydroxyl free radical, •OH, to improve photodynamic therapy, and the results have shown that this material can be used as an effective drug for the treatment of cancer due its properties such as photoluminescence, cheapness, and stability [151].

Additionally, a W chemical substitution in α-$Ag_2W_{0.75}Mo_{0.25}O_4$ has been described [147]. These solid solutions were prepared *via* the MAH [145, 147, 149] and CP [148] methods. Recently, the α-$Ag_2W_{0.75}Mo_{0.25}O_4$ solid solution has been synthesized in two steps: initially, the precipitated sample corresponds to the α-Ag_2WO_4/β-Ag_2MoO_4

heterostructure, and then, the posterior microwave irradiation favors the substitution of W^{+5} by Mo^{5+} cations and subsequent formation of the solid solution [147]. The results showed changes in the morphology and optical properties, and by tuning the TM concentration, simultaneous control of the optical and electronic properties can be achieved. This behavior enhances the photodegradation of methylene blue (MB) dye and tetracycline (TC) antibiotic [145] and RhB dye [147]. When the MAH [145, 147] method is used, in the samples obtained at the longest microwave irradiation time, the number of structural defects was increased. As an example, **Fig. 6** illustrates the α-Ag_2WO_4 structure with doping atoms at the W and Ag sites.

<Insert Fig. 6>

6. Ag_2WO_4 composites

6.1. *C-based compounds*

Coupling C-based materials, graphitic carbon nitride (g-C_3N_4), reduced graphene oxide (rGO), or transition metal carbides/nitrides (MXenes), with other semiconductor materials, have received considerable attention due to their excellent chemical stability and unique electronic structures. Particularly, these C-based materials with two-dimensional thin sheet structures retain this shape with wrinkled regions after hybridizing with Ag_2WO_4. This morphology might provide enough contact surface area between them and the Ag_2WO_4 particles and can facilitate charge-carrier transport. The Ag_2WO_4/g-C_3N_4

composites can typically be prepared by a simple deposition-precipitation method (or *in-situ* Ag_2WO_4 growth on the g-C_3N_4 surface) at room temperature [152-156]. The most interesting result of this procedure is that the orthorhombic α-Ag_2WO_4, the thermodynamically most stable phase, is not observed, and diffraction peaks indexed according to the hexagonal β-Ag_2WO_4 phase, thermodynamically less stable, are obtained. The addition of g-C_3N_4 nanosheets plays an important role in controlling the phase structure of Ag_2WO_4. After adsorbing the precursor ions, the g-C_3N_4 nanosheets can provide active sites for the nucleation and growth of β-Ag_2WO_4 NPs, and the phase transformation from β-Ag_2WO_4 to stable α-Ag_2WO_4 can effectively be inhibited because precursor ions are tightly tiled onto the g-C_3N_4 nanosheets [154, 155]. These results are in correspondence with previous reports where β-Ag_2WO_4 crystals, synthesized using a simple precipitation method, are generally obtained using templates, such as polymethacrylic acid [93], polyvinyl pyrrolidone [98], and acrylamide [33]. When Ag_2WO_4 supported on g-C_3N_4 is synthesized by the same precipitation route, but additional SC impregnation is used, the β-Ag_2WO_4 is obtained, but extra diffraction peaks appear, which are assigned to α-Ag_2WO_4 [157]. Similarly, when at the final step of Ag_2WO_4/g-C_3N_4 synthesis, the precursor mixture is transferred into a Teflon-lined autoclave and subsequently hydrothermally heated (at 180 °C for 12 h) [158] or warmed at 300 °C for 2 h [159], pure α-Ag_2WO_4, as the only Ag_2WO_4 phase in the composite, is obtained. These synthetic routes, assisted by additional energy, sonochemical or thermal, provide adequate conditions for partial or total phase transformation to the thermodynamically more stable α-Ag_2WO_4. Furthermore, this procedure can achieve the growth of Ag NPs on the Ag_2WO_4 surface and the ternary composite Ag/Ag_2WO_4/g-C_3N_4 [159]. In addition, quaternary

Ag_2WO_4-based g-C_3N_4-containing composites have been reported recently [160], and the corresponding results proved that multicomponent heterostructures are a promising strategy to promote the photocatalytic performance of Ag_2WO_4.

A ternary Fe-doped g-C_3N_4/Ag_2WO_4 visible light active photocatalyst with exceptional RhB degradation was fabricated by Alosaimi et al. through an ultrasonic-assisted facile hydrothermal method [161]. By using the solvothermal method, Vinoth et al have obtained a novel Ag_2WO_4 nanorod encapsulated sulfur-doped graphitic carbon nitride (Ag_2WO_4@SGCN). According to the authors, this material was successfully applied for the electrochemical detection of nitrofurantoin, revealing its practical applicability for sensing [162].

Recently, graphene oxide (GO) and Ti_3C_2, with a two-dimensional sheet structure, were successfully used on GO/Ag_2WO_4 [163], GO/Ag_2O/Ag_2WO_4 [164], and Ag_2WO_4/Ti_3C_2 [165] composites. The diffraction peaks of the Ag_2WO_4 pattern can be assigned to crystal planes of the α-phase of Ag_2WO_4 crystals. Again, the hydrothermally assisted route provides favorable conditions for producing the most stable Ag_2WO_4 phase. On the other hand, as expected by the CP method, the combination of two-dimensional (2D) Ti_3C_2 with Ag_2WO_4 produced an Ag_2WO_4 sample in good agreement with the hexagonal phase β-Ag_2WO_4 [165]. In addition, an Ag_2WO_4/GO-based nanocomposite has recently been SC synthesized with a suitable electrochemical performance as a potential material for supercapacitor electrodes [166]. By analysis of the images from TEM for the C-based compounds with Ag_2WO_4 composites, several morphologies, such as irregular sphere-like [152, 154, 165], nanorod [157, 158], spindle-like [153], and rod-like [163, 167]

morphologies, can be observed. All these composites have been successfully applied to several photocatalytic degradation processes of organics (dyes, antibiotics, and so on) for environmental remediation. In addition, other interesting abilities such as antibacterial disinfection [153, 155, 168] have also been reported.

6.2. *Chalcogenides*

Some chalcogenide compounds, such as Ag_2S, WS_2, MoS_2, VS_4, ZnS, MnS, and Sb_2S_3, have also been used in composites with Ag_2WO_4. These compounds behave as semiconductors with a band gap between 1-2 eV, exhibiting excellent performance in charge separation, accelerating electron transfer, and high redox ability.

A series of Ag_2S/Ag_2WO_4 composites were synthesized with different Ag_2S compositions via a facile successive precipitation route [169]. For the Ag_2S/Ag_2WO_4 composites, the main characteristic diffraction peaks of Ag_2WO_4 can be indexed according to pure α-Ag_2WO_4. From a morphological point of view, α-Ag_2WO_4 appears with a regular microrod, and on their surface, regular NP-Ag_2S are deposited. On the other hand, for a facile SC method, Ag_2S/Ag_2WO_4 (denoted as U-Ag_2S/Ag_2WO_4) was also obtained [170] and compared with Ag_2S/Ag_2WO_4 composites fabricated by the precipitation method. A similar orthorhombic α-Ag_2WO_4 phase with more evident changes in morphology can be observed. Ultrasonic irradiation yields an evident improvement in surface area in connection with the decrease in the average crystallite size of the samples, which could indicate that ultrasonic irradiation improved the dispersion and decreased the crystallite sizes. The attached NP-Ag_2S are fused into fluffy particles. In addition, a rod-like (typical

hexagonal submicron-rod) α-Ag_2WO_4 crystal with Sb_2S_3 chalcogenide nanorods on its surface was prepared by a simple wet impregnation method [171]. This heterostructure exhibits prolonged visible light absorption when compared to pure α-Ag_2WO_4.

2D chalcogenides, such as MoS_2 and WS_2, have also been used to join Ag_2WO_4 in composites. A MoS_2/Ag_2WO_4 nanohybrid was prepared *via* the hydrothermal method on a Teflon-lined autoclave heated at 180 °C for 24 h [172]. Instead, the Ag_2WO_4/WS_2 composites [167] were fabricated by using a deposition-precipitation method in a similar procedure to composites of Ag_2WO_4 with 2D g-C_3N_4 [152-154]. The XRD patterns of MoS_2/Ag_2WO_4 and Ag_2WO_4/WS_2 were consistent with all the diffraction peaks of the orthorhombic α-phase and hexagonal β-phase of Ag_2WO_4, respectively, in agreement with the observed report for 2D g-C_3N_4. By a simple *in-situ* deposition-precipitation method, the sheet morphology can provide active sites for the nucleation and growth of metastable β-Ag_2WO_4 in which precursor ions are tightly tiled onto the nanosheets, and the phase transformation from β- to stable α-Ag_2WO_4 can effectively be inhibited. On the other hand, the synthesis routes assisted by additional energy, SC and hydrothermal, are thermodynamically favorable for the synthesis of the most stable α-Ag_2WO_4 polymorph. Recently, Sudheer et al. developed VS_4/Ag_2WO_4 [173], ZnS/Ag_2WO_4 [174], CoS/Ag_2WO_4 [175], and MnS/Ag_2WO_4 [176] composites synthesized through the CP method, and the orthorhombic phase of Ag_2WO_4 was obtained. These composites presented highly efficient photocatalysis activity for the removal of pollutants (MB degradation) from water and as excellent antimicrobial agents (for *E. coli* and *Bacillus subtilis* – *B. subtilis*).

The overall morphology for these composites of the Ag_2WO_4 crystals with 2D materials prepared by *in-situ* deposition-precipitation clearly shows that the Ag_2WO_4 particles were grown over the 2D nanosheet. Initially, the Ag precursor is introduced into the 2D-material suspension, and Ag^+ cations can be tightly adsorbed onto the surface of the nanosheets through electrostatic interactions. Upon the addition of the W precursor, Ag^+ cations react with WO_4^{2-} complex anions and Ag_2WO_4 nuclei are generated. Finally, the Ag_2WO_4 particles grow directly on the sheet surfaces. This growth strategy is schematically illustrated in **Fig. 7**.

<Insert Fig. 7>

Regarding the optical behavior of Ag_2S/Ag_2WO_4, U-Ag_2S/Ag_2WO_4, and Ag_2WO_4/WS_2 composites, the absorption edge of the ultraviolet-visible (UV–Vis) spectra shows a slight redshift and an increase in the visible light absorption when compared to pure Ag_2WO_4 crystals. Additionally, from photoluminescence (PL) measurements, the peak intensity in the composites is much weaker than that of pure Ag_2WO_4 crystals, indicating the importance of the efficiency of charge carrier separation for the composites.

6.3. *Halogens*

The AgX (X = Cl, Br, I) family is one of the most important Ag-based efficient visible-light-driven photocatalysts, attracting much attention. It is well known that these compounds are easily decomposed to generate, after light irradiation, hybrids with metallic Ag, which have been used as highly efficient plasmonic photocatalysts owing to the surface

plasmon resonance (SPR) effect [177-180]. Consequently, the production of AgX/Ag_2WO_4 [27, 40, 61, 98, 181-186] binary composites is an effective approach to photocatalyst design for practical applications in solving existing environmental problems. Initially, by a facile precipitation process, Ag_2WO_4 particles can be obtained with a high yield at room temperature. Subsequently, AgX crystals are grown on the surface of Ag_2WO_4 to form Ag_2WO_4/AgX composites by a facile *in-situ* anion exchange reaction with different X^- ion solutions at room temperature. The results revealed that the Ag_2WO_4 rod-like structure acted as the template of 1D AgX/Ag_2WO_4 heterocrystals. These 1D semiconductor structures demonstrated substantial catalytic efficiency due to the high aspect ratio, which enhanced light absorption, rapid electronic transport along the long axis, and efficient utilization of electron-hole pairs.

In the Ag_2WO_4/AgX hybrid nanorods, all the α-Ag_2WO_4 crystals with well-indexed diffraction peaks according to the orthorhombic structure joined to typical peaks of the face-centered cubic phases of AgCl and AgBr and the hexagonal AgI phase, indicating the successful formation of the composite structures. Interestingly, the β-Ag_2WO_4 crystals are stabilized in AgBr/β-Ag_2WO_4 heterostructures when cetyltrimethylammonium bromide is used as the AgBr precursor [185]. The FE-SEM image of the as-prepared composite consisted of uniform rod-like morphologies for Ag_2WO_4, while the AgX nanocrystals were uniformly dispersed on the surface of Ag_2WO_4. The formation of the Ag_2WO_4@AgX core@shell or heterostructure is evident for some composites [26, 27, 40, 182]. A schematic procedure for the synthesis and final microstructure is shown in **Fig. 8**.

<Insert Fig. 8>

For all Ag_2WO_4/AgX hybrid nanorods, a pronounced enhancement in the visible-light absorption range and an absorptive capability stronger than that of Ag_2WO_4 are clearly observed in the UV–vis diffuse reflection spectra [40, 98, 182]. This enhancement in the optical property was achieved when the AgX content was progressively increased. Notably, among all AgX hybrids, the Ag_2WO_4/AgBr composite shows a much stronger response in the visible region. The AgX/Ag_2WO_4 heterojunctions can improve the visible light response of Ag_2WO_4 crystals, and thus, they can be expected to be efficient visible-light-driven photocatalysts. Through the appropriate procedure (mostly by photoirradiation), some of these binary composites are transformed into Ag/AgX/Ag_2WO_4 ternary composites [27, 61, 181, 183]. In addition to the advantages already mentioned for similar binary systems, the highly enhanced performance of the Ag-modified AgX/Ag_2WO_4 hybrid can be attributed to the SPR effects of metallic Ag NPs. Ag^0 growth from AgX/Ag_2WO_4 in the nanometer range increases the total surface area and improves the synergistic effects, which can effectively suppress the recombination of photo-induced electrons and holes.

Additionally, these Ag-based binary systems were used to improve the structural/optical performance of several semiconductor oxides, producing multicomponent composites for enhancing the photocatalytic behavior of these oxides [184, 187, 188]. Ag_2WO_4-AgX (X = Cl, Br, I)-sensitized TiO_2 nanotubes (NTs) arrays (TiO_2 NTs were prepared by two-step anodization of Ti foils) were prepared *in-situ* by successive ionic layer adsorption and reaction deposition of Ag_2WO_4 NPs on TiO_2 NTs [187]. The as-prepared TiO_2 NTs/Ag_2WO_4 was immersed into X^- solution, and by ion-exchange

hydrothermally assisted (180 °C for 3 h), TiO_2 NTs/Ag_2WO_4-AgX (X = Cl, Br, I) heterojunctions were formed. Similarly, TiO_2 NPs were used in this method (*in-situ* preparation by successive ionic layer adsorption and reaction deposition) to prepare TiO_2/Ag_2WO_4/AgBr nanocomposites by the ionic exchange in a suspension refluxed at 96 °C for 15 min [188]. Also, by this multi-step procedure, the ZnO/Ag/Ag_2WO_4/AgI, with additional photoirradiation [189] and TGCN/Ag/Ag_2WO_4/AgI (TGCN=tubular g-C_3N_4) [190], quaternary composites were obtained and used for photocatalytic removal of MB, methyl orange (MO), and fuchsine dyes; and antibiotics such as TC and amoxicillin, under visible-light illumination using Ag_2WO_4 for environmental applications.

6.4. *Ag_2WO_4 composites with metal oxides and metal-organic compounds*

A particularly interesting strategy for preparing Ag_2WO_4-based composites is mixing with magnetic oxides. It should be noted that after coupling with Ag_2WO_4, the magnetic behavior of these oxides is still retained, which suggests a potential aptness of the composites for magnetic separation and recovery using a magnet.

Based on this strategy, binary (Ag_2WO_4/Fe_3O_4) [191], ternary (Ag/β-Ag_2WO_4/$CoFe_2O_4$, Ag_2WO_4@ZnO@Fe_3O_4 and SiO_2/Fe_3O_4/Ag_2WO_4) [192-194] and quaternary (g-C_3N_4/Fe_3O_4/Ag_2WO_4/AgBr and Fe_3O_4@SiO_2@Ag_2WO_4@Ag_2S) [195, 196] systems have been studied. The Fe_3O_4/Ag_2WO_4 nanocomposites were obtained through facile routes with cubic Fe_3O_4 and β-and α-Ag_2WO_4. Images clearly show that Fe_3O_4 particles are randomly attached to the surface of Ag_2WO_4 nanorods. For the ternary systems, $CoFe_2O_4$ and ZnO/Fe_3O_4 solutions were previously dispersed, and then the

solutions of Ag_2WO_4 precursors were subsequently mixed. The $Ag_2WO_4/CoFe_2O_4$ composite (a flower-like morphology) was finally irradiated under a halogen lamp to obtain the $Ag/Ag_2WO_4/CoFe_2O_4$ ternary composite. At the same time, the $Ag_2WO_4/ZnO/Fe_3O_4$ was transferred into a Teflon-lined autoclave and heated at 140 °C for 2 h. As expected, by the simple deposition/precipitation route (to obtain $Ag/Ag_2WO_4/CoFe_2O_4$) and by the hydrothermal route (to obtain $Ag_2WO_4/ZnO/Fe_3O_4$), β-Ag_2WO_4 and α-Ag_2WO_4, respectively, were revealed by XRD. The g-$C_3N_4/Fe_3O_4/Ag_2WO_4/AgBr$ quaternary composite was prepared by the refluxing method. For this route, β-Ag_2WO_4 with a hexagonal structure appeared in the nanocomposite. The magnetic properties were measured, and it should be noted that the magnetic behavior of the oxides is still retained after coupling in the composite. However, due to the presence of a nonmagnetic Ag_2WO_4 counterpart in the composite, the magnetic parameter values are much lower than that of pure magnetic oxide. These results confirm that the composites can be a recoverable material, magnetically collected and reused.

On the other hand, nonmagnetic semiconductor oxides have also been used in composites joined to Ag_2WO_4. TiO_2, WO_3, and ZnO are among the common oxide materials used due to their good physical and chemical stability, non-toxicity, and excellent optics, biology, and photochemistry properties. However, these pure oxides are problematic due to their relatively wide band gap and high recombination rate for photoexcited charge carriers. Hence, it is necessary to tune this characteristic to enhance efficiency in diverse applications, and the oxide/Ag_2WO_4 composite has been used for this purpose. Composite systems with simple oxides such as $Ag/(ZnO,Mn_3O_4,WO_3)/Ag_2WO_4$ [197-204], β-

Bi_2O_3/Ag_2WO_4 [205], $MnWO_4/Ag_2WO_4$ [206], Ag_2WO_4/CeO_2 [207], α-Ag_2WO_4/Ag_3PO_4 [208], CoO-Ag_2WO_4 [209, 210], $ZnBi_2O_4/Ag_2WO_4$) [211], and $Ag_2WO_4/(TiO_2,ZnO)/AgX$ (X = Cl, Br, I) [187-189] have been obtained for diverse synthetic routes. These last three heterojunctions have been described in the present work in the section on composites with Ag_2WO_4 crystals and halogen-based materials. Other more complex oxides have also been used [212-220]. In short, some results on preparation methods, phases, and morphologies reported in previous works are summarized in **Table 1**. Most of these reports explore applications of photocatalytic properties (as seen in **Table 1**) due to the fact that the fabrication of Ag_2WO_4-based composites has proven to be an important research strategy for further enhancement of the photodegradation of organic pollutants.

Similarly, metal-organic framework (MOF) compounds have emerged as potential candidates to form composites with Ag_2WO_4 crystals. These metal complexes have interesting electron transfer abilities and a large number of derivatives, among other promising characteristics for several electronic and optoelectronic applications. Some reports of Ag_2WO_4 composites with these compounds [103, 221-223] are listed in **Table 1**.

<Insert Table 1>

In summary, the composite catalyst systems exhibit higher photoactivity than their respective single counterpart catalysts, which can be attributed to the excellent synergy effects. Among others, higher photoexcited electron-hole pair separation, ease of interfacial charge transfer, higher surface sensitivity, and excellent stability are essential characteristics for the successful application of Ag_2WO_4/oxide and Ag_2WO_4/metal-organic composites.

This formation of heterojunctions proves that it is a suitable strategy to improve several Ag_2WO_4 applications, such as the photocatalytic degradation of organic dyes, biocide activity, and others. The adequate energy bands match between Ag_2WO_4 and the other semiconductor reduced the free charges recombination in the composite, ascribed to the rapid and effective separation and transportation of the photogenerated electron-hole pairs, and also enhanced the photocorrosion inhibition with a small Ag_2WO_4 self-consumption. Further, it is worth pointing out that the addition of another semiconductor with a narrow band gap overcomes the low-efficiency Ag_2WO_4 in the utilization in visible light regions. When Ag_2WO_4/gC_3N_4 photocatalysts, for example, were exposed under visible light for degradation of RhB, a typical organic dyes pollutant, the photocatalytic degradation efficiency achieves optimal values that are >90% within 20-50 min under irradiation [152, 159, 224]. Similar efficient performances were obtained when Ag_2WO_4 is hybridized with silver halide, AgX (X = Cl, Br, I). The photocatalysis for the RhB dye showed that the $AgBr/Ag_2WO_4$ composite had the most notable photoactivity among them. The complete RhB degradation time is 0.5 h, while $AgCl/Ag_2WO_4$, AgI/Ag_2WO_4, and pure Ag_2WO_4 catalysts took about 2, 1.5, and 4 h, respectively [182]. Also, 100% of degradation efficiency at 60 min for $AgBr/Ag_2WO_4$ had been reported [185]. Other organics non-azo dyes have also been effectively degraded under visible light such as: MO with $g-C_3N_4/Ag_2WO_4$ [40, 152, 154], Ag_2S/Ag_2WO_4 [169] and Ag_2WO_4/MoS_2 [172]; and methyl blue (MB) with Ag_2WO_4/VS_4 [173], Ag_2WO_4-MnS [176], CoS/Ag_2WO_4 [175] and $AgCl/Ag_2WO_4$ [61]. Similarly, contaminating drugs such as indomethacin in $Ag_2WO_4/g-C_3N_4$ [156]; para-chlorophenol [40], and ceftriaxone, in AgI/Ag_2WO_4 [186], among others, underwent photochemical degradation under visible light.

In several works, photocatalytic disinfection efficiency of the excited photogenerated electron-hole pairs in the composite has strong oxidative capacities that could attack, inactivate and break the semipermeable cellular membrane and eventually result in cell death. This enhanced visible light antibacterial activity has been reported against *E. coli* in g-C_3N_4/Ag_2WO_4 [153, 155]; and for *E. coli* and *B. subtilis* for several composites of Ag_2WO_4 hybridized with chalcogenides based-compounds [153, 173-175].

In terms of the successful heterojunction design, several aspects must be taken into consideration according to the suitable bands (VB and CB) alignment of the adjacent semiconductors [225, 226]. In particular, for the Ag_2WO_4 composites, the Z-scheme heterojunction [154-156, 167, 185, 199, 227-230] and conventional type II heterojunction [169, 205, 207, 211, 213, 224] are the most employed. A schematic representation of both types of Ag_2WO_4 heterojunctions is displayed in **Fig. 9**.

<Insert Fig. 9>

Journal Pre-proof

7. Interaction with electrons and laser

Electrons and electromagnetic radiation interact with matter and can change the physical and chemical properties of a material. Therefore, techniques such as EB and fs laser irradiation have emerged as modern, clean, and efficient tools for tuning material properties. FE-SEM and TEM microscopes have recently been employed as EB sources to produce metal NPs on the surfaces of semiconductor materials. At the same time, it is

possible to observe the *in-situ* growth of these NPs and the phenomena involved. Different metal NPs, such as Au, Cu, Li, Co, and others, have already been generated on the surfaces of semiconductor materials by this technique [231-236]. Ag NPs are well known for their attractive properties, and their growth on the surface of Ag-based semiconductors can improve some properties, such as antimicrobial activity, gas sensing, and photocatalysis. Thus, several studies have been published related to the growth of Ag NPs stimulated by EB irradiation on the surfaces of Ag-based ternary oxides, such as Ag_2WO_4, β-Ag_2MoO_4, Ag_3PO_4, β-$AgVO_3$, and Ag_2CrO_4 [237-241].

Irradiation of solids with energetic particles or light, such as electrons or lasers, typically gives rise to the formation of atomic defects in the target and spoils the material properties. The necessity to understand the irradiation-induced processes was the initial driving force for studying the effects of irradiation on solids. Recently, great advances in nanoscience and nanotechnology fields have been made due to the expansion and diffusion observed employing TEM and high resolution (HR)-TEM images, which is possible using TEM heating holders for *in-situ* electron microscopy [242-246]. However, new *in-situ* observations of the crystal growth of different materials from TEM [247, 248] and *in-situ* liquid TEM have shed light on understanding the growth process of copper and lead sulfide nanostructures [249-251]. Moreover, the growth mechanisms of some nanomaterials can be observed simply through the watchful eyes of the researcher and microscopist [252], without the use of extra accessories under the microscope [253, 254]. This point is of great relevance to disseminating this new method of investigating the stages of the crystal growth process due to the possibility of observing all evolution step-by-step at the nanoscale [255,

256]. In general, several works have been reported using TEM heating holders to monitor the growth process of different nanomaterials, such as bismuth [257], germanium [258], indium-arsenide [259], and vanadium oxide [260]. Moreover, for the first time, our research group [18, 20, 31, 113, 261] observed the *in-situ* growth of metallic Ag nanorods from α- and β-Ag_2WO_4 crystals with unstable surfaces through FE-SEM images without a heating holder, as shown in **Figs. 10(a-c)**.

<Insert Figs. 10(a–c)>

A series of *in-situ* FE-SEM images were acquired during Ag NP growth from the unstable surface of α-Ag_2WO_4 crystals at 30 kV without a heating holder. **Fig. 10(a)** illustrates an initial FE-SEM image of α-Ag_2WO_4 crystals, which was acquired soon after rapid approach and focus adjustment. These crystals have a hexagonal rod-like elongated shape (**Fig. 10(a)**) and were modeled from the crystallographic data presented. These crystals are formed rapidly by mixing Ag^+ cations and WO_4^{2-} ions into a hot aqueous solution (90 ºC). This synthesis method promotes fast kinetics of nucleation and the growth of α-Ag_2WO_4 crystals. **Fig. 10(b)** shows that when these crystals under a high vacuum (1×10^{-5} Pa) are exposed to electrons provided by a microscope after 6 min, it is possible to observe the growth process of metallic Ag NPs on the hexagonal rod-like α-Ag_2WO_4 crystals. After the α-Ag_2WO_4 crystals receive a reasonable amount of electrons, the appearance of several surface defects can be noted due to the mobility of metallic Ag NPs to the surface of α-Ag_2WO_4 crystals, as illustrated in **Fig. 10(b)**. Several FE-SEM experiments and the corresponding images demonstrate that the growth process of metallic Ag nanorods is highly reproducible. In **Fig. 10(b),** it can be observed a large amount of

metallic Ag nanorods formed on the surface of the α-Ag_2WO_4 crystals after 10 min of exposure to electrons from the microscope. Due to this EB process, a structural transformation or symmetry break of the orthorhombic structure occurs, resulting in the *in-situ* formation of Ag^0 nanorods and defects in the α-$Ag_{2-x}WO_4$ crystals. We have modeled this EB process and the growth of these metallic Ag^0 nanorods with the formation of disordered α-$Ag_{2-x}WO_4$ crystals based on FE-SEM images (**Fig. 10(b)**). Tsuji et al. [262] monitored the rapid transformation of various Ag nanostructures using the chemical reduction method from Ag^+ cations to Ag^0. However, the EB process uses only electrons from the microscope to promote the reduction of angular [AgO_2] clusters present in α-Ag_2WO_4 crystals to metallic dodecahedral [$AgAg_{12}$] clusters. Finally, in **Fig. 10(c)**, a significant change in the α-Ag_2WO_4 surface utilizing energy-dispersive X-ray (EDX) imaging can be noted by mapping Ag-L3, which is due to the formation of Ag^0 NPs at other regions of α-Ag_2WO_4 crystals through an absorption process of some Ag^0 NPs and amorphization of part of the orthorhombic structure of α-Ag_2WO_4.

7.1. *The growth of Ag NPs on Ag_2WO_4 crystals by electron beam irradiation*

The *in-situ* growth of Ag NPs on the surface of α-Ag_2WO_4 under an accelerated EB from a high *vacuum* electron microscope was reported for the first time by our group in 2013. A sample of α-Ag_2WO_4 was illuminated inside a TEM operated at 200 KV, and images of different moments of exposition, with intervals of 5 seconds, were registered. They observed Ag filaments growing on the semiconductor surface, with posterior reabsorption within time. They also observed these phenomena with an SEM microscope,

but the process was slower and less intense in this case. However, in SEM and TEM, the NPs grow relatively quickly, with just a tiny electron dose used to focus the image [12]. Several subsequent studies from our group investigated the growth of Ag NPs on the Ag_2WO_4 surface from the EB irradiation via *in-situ* analysis using SEM and TEM, combined with theoretical calculations. One of them reported the influence of the synthesis method on growth characteristics, suggesting that order-disorder structural parameters influence nanocrystal growth [17]. Ag_2WO_4 is an *n*-type semiconductor, and with EB irradiation, randomly distributed Ag vacancies form in the crystal. This phenomenon produces *p*-type defects in the structure, creating a new intrinsic *n*/*p*-type semiconductor with novel properties. This fact was confirmed when an exponential increase in the bactericidal property was observed with the *n*-type semiconductor, as shown in another publication [19].

The early events related to the nucleation of Ag filaments on α-Ag_2WO_4 crystals, driven by the EB microscope under a high *vacuum*, were studied in detail by our research group using a combination of theory, computation, and experiments. These studies demonstrated that the Ag nucleation and formation on α-Ag_2WO_4 crystals is a result of order/disorder effects generated in the crystal by EB irradiation, associated with structural and electronic changes of the angular [AgO_2] clusters and distorted tetrahedral [AgO_4] clusters and, to a minor extent, to the distorted octahedral [WO_6] clusters, which collectively represent the constituent building blocks of the α-Ag_2WO_4 [18]. To further investigate and understand the phenomena involved in the growth of Ag NPs on α-Ag_2WO_4 crystals, another combined experimental and theoretical study was performed using *in-situ*

SEM and TEM images and density functional theory. The EB irradiation by using SEM was generated at four different electron voltages (5, 10, 15, and 20 kV), whereas TEM images were obtained at 200 kV. The main contributions of that work were that first, the start of Ag NP growth occurs in a few seconds of exposure to the EB independent of the voltage, although there is an increase in the number of NPs for higher voltages; and second, the Ag centers at the (100) surface suffer a decrease in the activation barrier for diffusion processes with the injection of electrons [20]. Other mechanistic aspects of the formation of Ag NPs by EB irradiation were discussed by our research group [263] and a review on the topic was also published later [264].

Despite all these studies related to the growth of Ag NPs on α-Ag_2WO_4, the description of the atomic and electronic structure of the semiconductor irradiated by electrons remained unclear until our recent work [261]. This study concluded that there is a predominant growth of Ag on the (100) surface of α-Ag_2WO_4, where Ag^0 species (with different coordination numbers) can diffuse out of the surface with a very low energy barrier (less than 0.1 eV). Thus, they initiate the growth of metallic Ag nanostructures and leave Ag vacancies in the bulk material, which increases the structural disorder of α-Ag_2WO_4 crystals and their electrical resistance [261]. The morphological evolution of Ag NPs in response to the EB passage was investigated in detail [265]. Different mechanisms were observed, such as mass transport, site-selective coalescence, structural rearrangement during and after coalescence or dissolution, and the evolution of the growth mechanism with surface faceting leading to a more stable configuration.

Additionally, the nature of the sintering process (the phenomena involved in the junction of the grain boundaries of two initially isolated particles that bond together to form larger NPs) of Ag NPs was unraveled at an atomic resolution for the first time [266]. This study concluded that the EB of TEM produces SPR in the Ag, forming neutral nanoelectric dipoles responsible for the coalescence processes, which start with a disorder-driven pathway followed by a structural disorder-to-order transition *via* an oriented attachment mechanism. The resulting larger clusters are thus a consequence of these sintering processes controlled by dipole interactions [267].

Moreover, the dose-dependent effect (0, 2, 4, and 6 kGy from a variable energy accelerator) of EB irradiation on the structural and optical properties of α-Ag_2WO_4 NPs was studied by Sreedev *et al*. [268]. The findings reveal that EB irradiation induces particle size variation, increases strain, surface defects, optical band gap deviations, and PL and Raman spectra modifications, changing the optical and photoluminescent properties of α-Ag_2WO_4 [268]. Recently, for the first time, our research group [113] showed the presence of some silver oxides (Ag_2O and Ag_3O_4) close to the interface of the mother Ag_2WO_4 crystal, in addition to the predominance of metallic Ag in the extruded material from the electron-irradiated Ag_2WO_4, which suggests that the EB induced atomic diffusion of O and Ag species in the microcrystals. The *in-situ* formation, growth, and subsequent reabsorption of Ag NPs on the surface of the β-Ag_2WO_4 metastable phase was reported, for the first time, in 2016 [269]. After that, we examined the structural properties and electronic behavior of β-Ag_2WO_4 irradiated by an EB by joint an experimental and theoretical investigation. Based on the analysis of the evolution of geometry and electronic structure,

the Ag nucleation process takes place via the reduction of the Ag^{+} of the [AgO_6] and [AgO_5] clusters [31].

7.2. *Ag NP growth on Ag_2WO_4 by femtosecond laser irradiation*

The laser ablation of solids is a material processing technique that has received much attention from the scientific community over the last few years. The interactions of ultrafast pulses from a laser source with matter can also be an efficient tool for generating metal NPs, with the advantage of a more straightforward scale-up compared to the TEM or SEM electron beams. Although a few articles refer to laser ablation in liquid to modulate and enhance some properties of Ag_2WO_4 crystals, very recently, Lin et al. [30], report the use of laser ablation to generate Ag NPs on solid Ag_2WO_4.

The first paper on the production of Ag NPs on Ag_2WO_4 surfaces using fs laser irradiation was published in 2018 [3]. This study reported the novel formation of Ag NPs from α-Ag_2WO_4 by laser-assisted irradiation. The Ag NPs generated were spherical, isolated, or agglomerated, and they did not grow with increasing exposure time under the electron microscope, unlike what was observed in EB, as previously discussed. The authors attributed the short-pulse laser interaction with matter to a mechanism not fully understood but based mainly on the laser pulse energy absorption by the electrons on the sample's surface in an instantaneous practical process. Thus, the excitation of electrons contrasts with the basal state of the electrons in the lattice, which leads to an equilibrium that is reached through rapid electron-phonon interactions and electron diffusion out of the excited region. The ablation occurs when the excitation is high enough, which is different from the

EB irradiation process, which occurs in sequential steps. The fs laser-irradiated samples presented an improved bactericidal activity compared to the non-irradiated Ag_2WO_4 material.

The peculiar phenomena caused by the interactions of ultra-short laser pulses and matter generates unexpected or even non-equilibrium metastable materials. As an example, we have reported [270] the formation of a nanoalloy formed by Ag and Bi, which are immiscible in bulk. Still, the fs laser irradiation of a simple mixture of the precursors Ag_2WO_4 and $NaBiO_3$ obtained a random mixture of up to 6±1 atom % of Bi into the face-centered cubic structure of Ag. This partial Ag-Bi miscibility was also discussed recently from *ab initio* DFT calculations [271]. Another study reports a theoretical strategy based also on DFT and molecular dynamics simulations to investigate the effect of laser irradiation on semiconductor materials [272]. This methodology provides insights into the mechanisms of local disordering induced by the laser and conducting to the formation of metallic Ag clusters [273]. Irradiation of fs laser on α-Ag_2WO_4 provokes a 64-fold enhancement in the bactericidal activity, mainly due to the generation of metastable hexagonal Ag^0 on the surface of the material [110].

In summary, the efficiency of both novel techniques in the generation of new or enhanced materials was shown very recently by the application of (micro, nano)composites of Ag_2WO_4 and Ag NPs synthesized by EB and fs irradiation against tumor cells, both having enhanced effects against these tumor cells *via in vitro* assays, reassuring the importance of both tools in the superior material production [4]. Moreover, a very recent study demonstrated unconventional magnetic effects on Ag_2WO_4 by these irradiation

techniques, which opens the possibility for further explorations [274]. Also, the influence of morphology, surface band gap, and microstructure on the photoluminescence emissions of α-Ag_2WO_4 samples obtained by the CP method, followed by treatment with MAH at different synthesis times and two different irradiation processes, EB and fs laser, has been experimentally and theoretically investigated [275].

Fig. 11 presents a timeline (from 1973 until 2022) highlighting the key milestones and advances in the synthesis and applications of α-, β-, and γ-Ag_2WO_4 polymorphs.

<Insert Fig. 11>

Journal Pre-proof

8. Summary and future work

Ag_2WO_4-based materials have seen rapid growth in the last few years, with new examples of the different types and new applications being reported more frequently. As the field progresses, it can also be envisioned that structure and electronic properties are responsible for a wide range of technological applications. To enable their widespread practical usage, significant efforts have been devoted to finding relationships among the nature of chemical bonds, geometrical arrangements, and their unique properties. This review summarizes their rich history and highlights the contemporary relevance for assessing the most important properties and applications of Ag_2WO_4-based materials, as well as the fundamentals and recent progress of Ag_2WO_4 as multifunctional materials. To this end, new concepts and innovative strategies are discussed in detail. Special emphasis is devoted

to synthesis methods. Overall, this review article aims to help materials science chemists and physicists select suitable methods and techniques for the synthesis and characterization of semiconductor Ag_2WO_4-based materials and potentially other relevant materials. However, the changes in the local coordination of Ag and W cations and their electronic structure are difficult to observe directly by experimental methods. The combination of the results derived from experimental and first-principles calculations is a feasible strategy for studying these materials and should be efficiently transformed into a potent tool to explain and rationalize the properties and affordable applications. Widely spread crystal lattices of Ag_2WO_4 polymorphs represent a natural flexible platform for the chemical design of various advanced functional materials with unique features.

The photocatalytic efficiency could be improved by morphology control to obtain superior performance, which provides more active sites for the corresponding reaction. In this strategy, various additives, solvents, and surfactants are used to fabricate Ag_2WO_4-based materials with controlled morphology. The synthetic methods and the photocatalytic behavior of numerous morphologies were introduced systematically. Our thorough analysis of the geometric structure, morphology and electronic and optical properties of Ag_2WO_4 polymorphs reveals fundamental insights into their chemistry and shows high variability that can be used to justify and guide additional experimental investigation into this complex material. The interaction between electrons/lasers and matter promotes major changes, such as the growth of Ag NPs in Ag_2WO_4-based materials. This work reviews the ultimate applications of Ag_2WO_4-based materials when exposed to EB and *fs* laser irradiation, leading to the enhancement of photocatalytic and bactericidal activities. This review serves

the purpose of informing researchers in this interdisciplinary field about a unique approach based on the combination of theory, simulation, and experiments. We hope that this study will provide valuable information and inspiration for the study of Ag_2WO_4-based materials and that future advances will drive rapid development in this field. This roadmap will prove to be valuable both as a collective self-analysis of the materials science community, providing an updated picture, and as a dissemination tool, helpful to whoever is willing to spread knowledge and thus draw both new young scientists and further public and private resources to this exciting field of research.

From our viewpoint, future research needs to focus on the exploration of the formation of reactive oxygen species (ROS) over semiconductor surfaces is a topic of tremendous scientific attention owing to their essential role in photocatalytic and biological processes. In particular, the activation of both molecular oxygen, O_2, and water, H_2O, molecules is a fundamental step in almost all oxidation reactions involving ROS formation, including water treatment and photodegradation of pollutants due to their high chemical reactivity. Since ROS generation occurs on the surface of semiconductors, its efficiency is related to surface electronic and structural features. Specific chemical composition and crystal arrangements at the atomic level may contribute to the different performances. Therefore, precise design to balance the advantage of active sites at the morphology remains challenging. A comprehensive understanding of the mechanisms governing the nature of the active sites at the morphology of the materials thus entails a description of the defective states at the exposed surfaces in terms of their concentration, local structure, and spatial distribution since all of these affect the chemistry that the material is able to drive.

Inspired by the present results, high-throughput screening, machine learning, and computational materials design can guide for developing synthesis methods of Ag_2WO_4-based materials, thereby shortening the experimental period, reducing the workload, and saving experimental costs. In other fundamental studies, combining experiment and theory represents a promising research field for understanding the principles of activity, screening alternative high-performance and to develop advanced techniques for large-scale production.

Finally, the benefits of these materials for utilization in the fields of energy, environment, catalysis, and biological sciences are consistently analyzed, and several perspectives are presented. Nonetheless, since the biological properties of Ag_2WO_4-based nanomaterials nanoparticles are still in their infancy, future detailed *in vitro* and *in vivo* studies to assess the detailed biocompatibility of these nanoparticles are warranted. Hence, more examinations are expected to investigate their tunable properties and performance in interdisciplinary science. Moreover, a future perspective is also provided to shed light on the development of highly efficient Ag_2WO_4-based material. At the same time, their revealed architecture, chemistry, and morphological requirements allow us to believe that these materials will come into commercial use; at least, it is a prediction to optimistically believe. Most of the studies on the technological applications of Ag_2WO_4-based materials are limited to laboratory research, and more efforts are still needed to advance their practical use. Indeed, these and related materials are analyzed, and several possible research directions for overcoming the challenges are proposed to facilitate further research and development. Further efforts are expected to propel this exciting field forward. We hope the

discussions are of general interest and will stimulate additional developments for the next generation of advanced materials related to Ag_2WO_4 materials to help push the field forward in meaningful directions.

Acknowledgments

A.F.G. acknowledges the Universitat Jaume I for the postdoctoral contract (POSDOC/2019/30), Generalitat Valenciana for the exterior research grant (BEST/2021/048) and Fundação de Amparo à Pesquisa do Estado de São Paulo – FAPESP (2019/01732-1). J.A. acknowledges Universitat Jaume I (project UJI-B2019-30), the Generalitat Valenciana (Project AICO/2020/329), and the Ministerio de Ciencia, Innovación y Universidades (Spain) (project PGC2018094417-B-I00) for financially supporting this research. This work was also funded in part by FAPESP (2013/07296-2; 2016/23891-6; 2017/19548-7; 2017/26105-4), Financiadora de Estudos e Projetos – FINEP, Conselho Nacional de Desenvolvimento Científico e Tecnológico – CNPq (312318/2017-0 and 408036/2018-4), and CAPES.

Journal Pre-proof

References

1. Adhikari, S. *Samsung, TSMC Appeal For The $52 Billion US Chip Program*. 2022 [cited 2022 11/05/2022]; Available from: https://www.androidheadlines.com/2022/03/samsung-tsmc-52-billion-dollars-us-chip-program.html.
2. AFP. *Europa prepara gigante plano de investimento em semicondutores*. 2022 [cited 2022 11/05/2022]; Available from: https://exame.com/negocios/europa-prepara-gigante-plano-de-investimento-em-semicondutores/.
3. Assis, M., et al., *Towards the scale-up of the formation of nanoparticles on alpha-Ag2WO4 with bactericidal properties by femtosecond laser irradiation.* Sci. Rep., 2018. **8**: p. 1884.
4. Assis, M., et al., *Ag Nanoparticles/α-Ag2WO4 Composite Formed by Electron Beam and Femtosecond Irradiation as Potent Antifungal and Antitumor Agents.* Sci. Rep., 2019. **9**(1): p. 9927.
5. Chen, H. and Y. Xu, *Photoactivity and stability of Ag2WO4 for organic degradation in aqueous suspensions.* Appl. Surf. Sci., 2014. **319**: p. 319-323.
6. da Silva, L.F., et al., *A novel ozone gas sensor based on one-dimensional (1D) alpha-Ag2WO4 nanostructures.* Nanoscale, 2014. **6**(8): p. 4058-4062.
7. da Silva, L.F., et al., *Acetone gas sensor based on alpha-Ag2WO4 nanorods obtained via a microwave-assisted hydrothermal route.* J. Alloys Compd., 2016. **683**: p. 186-190.
8. de Foggi, C.C., et al., *Tuning the Morphological, Optical, and Antimicrobial Properties of alpha-Ag2WO4 Microcrystals Using Different Solvents.* Cryst. Growth Des., 2017. **17**(12): p. 6239-6246.
9. De Santana, Y.V.B., et al., *Silver Molybdate and Silver Tungstate Nanocomposites with Enhanced Photoluminescence.* Nanomater. Nanotechnol., 2014. **4**: p. 22-31.
10. Cui, X.J., et al., *Selective synthesis and characterization of single-crystal silver molybdate/tungstate nanowires by a hydrothermal process.* Chem. Eur. J., 2004. **10**(1): p. 218-223.
11. Cavalcante, L.S., et al., *Cluster coordination and photoluminescence properties of alpha-Ag2WO4 microcrystals.* Inorg. Chem., 2012. **51**(20): p. 10675-87.
12. Longo, E., et al., *Direct in situ observation of the electron-driven synthesis of Ag filaments on alpha-Ag2WO4 crystals.* Sci. Rep., 2013. **3**: p. 1676.
13. Dutta, D.P., et al., *High Adsorption Capacity for Cationic Dye Removal and Antibacterial Properties of Sonochemically Synthesized Ag2WO4 Nanorods.* Eur. J. Inorg. Chem., 2014. **2014**(33): p. 5724-5732.
14. Tang, J.W. and J.H. Ye, *Correlation of crystal structures and electronic structures and photocatalytic properties of the W-containing oxides.* J. Mater. Chem., 2005. **15**(39): p. 4246-4251.
15. Zhang, R., et al., *Facile hydrothermal synthesis and photocatalytic activity of rod-like nanosized silver tungstate.* Micro Nano Lett., 2012. **7**(12): p. 1285-1288.

16. Pan, L., L. Li, and Q. Zhu, *Facile synthesis of Co3O4 and Ag/Co3O4 nanosheets and their electrocatalytic properties.* J. Sol-Gel Sci. Techn., 2013. **67**(3): p. 573-579.
17. Longo, E., et al., *Toward an Understanding of the Growth of Ag Filaments on alpha-Ag2WO4 and Their Photoluminescent Properties: A Combined Experimental and Theoretical Study.* J. Phys. Chem. C, 2014. **118**(2): p. 1229-1239.
18. Andres, J., et al., *Structural and electronic analysis of the atomic scale nucleation of Ag on alpha-Ag2WO4 induced by electron irradiation.* Sci. Rep., 2014. **4**: p. 5391-5397.
19. Longo, V.M., et al., *Potentiated Electron Transference in alpha-Ag2WO4 Microcrystals with Ag Nanofilaments as Microbial Agent.* J. Phys. Chem. A, 2014. **118**(31): p. 5769-5778.
20. Pereira, W.d.S., et al., *Elucidating the real-time Ag nanoparticle growth on alpha-Ag2WO4 during electron beam irradiation: experimental evidence and theoretical insights.* Phys. Chem. Chem. Phys., 2015. **17**(7): p. 5352-5359.
21. Song, Q.-W., et al., *Efficient chemical fixation of CO2 promoted by a bifunctional Ag2WO4/Ph3P system.* Green Chem., 2014. **16**(3): p. 1633.
22. Guo, C.-X., et al., *Silver tungstate: a single-component bifunctional catalyst for carboxylation of terminal alkynes with CO2 in ambient conditions.* Green Chem., 2015. **17**(1): p. 474-479.
23. Pan, L., L. Li, and Y. Chen, *Synthesis and electrocatalytic properties of microsized Ag2WO4 and nanoscaled MWO4 (M=Co, Mn).* J. Sol-Gel Sci. Technol., 2013. **66**(2): p. 330-336.
24. Roca, R.A., et al., *Facet-dependent photocatalytic and antibacterial properties in α–Ag2WO4 crystals: Combining experimental data and theoretical insights.* Catal. Sci. Techn., 2015. **5**: p. 4091-4107.
25. Sreedevi, A., et al., *Nanophase α-Silver Tungstate for Potential Applications in Light Emitting Diodes and Gate Dielectrics.* Adv. Sci. Eng. Med., 2015. **7**: p. 498-505.
26. Wang, Q.P., et al., *Preparation of Fine Ag2WO4 Antibacterial Powders and Its Application in the Sanitary Ceramics*, in *Materials and Design, Pts 1-3*, X.M. Sang, et al., Editors. 2011. p. 1321-+.
27. Liu, X., et al., *Facile synthesis of Ag2WO4/AgCl nanorods for excellent photocatalytic properties.* Mater. Lett., 2013. **91**(0): p. 129-132.
28. Stone, D., et al., *Layered atomic structures of double oxides for low shear strength at high temperatures.* Scripta Mater., 2010. **62**(10): p. 735-738.
29. Vafaeezadeh, M. and M.M. Hashemi, *One pot oxidative cleavage of cyclohexene to adipic acid using silver tungstate nano-rods in a Bronsted acidic ionic liquid.* Rsc Adv., 2015. **5**(40): p. 31298-31302.
30. Lin, Z., et al., *Electronic Reconstruction of alpha-Ag2WO4 Nanorods for Visible-Light Photocatalysis.* ACS Nano, 2015. **9**(7): p. 7256-7265.
31. Roca, R.A., et al., *Formation of Ag Nanoparticles on beta-Ag2WO4 through Electron Beam Irradiation: A Synergetic Computational and Experimental Study.* Inorg. Chem., 2016. **55**(17): p. 8661-8671.

32. Galante, M.T., et al., *Silver Oxide-Based Semiconductors for Solar Fuels Production and Environmental Remediation: a Solid-State Chemistry Approach.* ChemElectroChem, 2019. **6**(1): p. 87-96.
33. Zhang, X.-Y., et al., *Construction of silver tungstate multilevel sphere clusters by controlling the energy distribution on the crystal surface.* CrystEngComm, 2015. **17**(5): p. 1129-1138.
34. Fadeeva, V.P., et al., *Determination of organogenic elements in the composition of functional compounds and materials.* J. Struct. Chem., 2014. **55**(5): p. 972-979.
35. Hu, B., et al., *Hierarchical silver indium tungsten oxide mesocrystals with morphology-, pressure-, and temperature-dependent luminescence properties.* Nano Res., 2010. **3**(6): p. 395-403.
36. Muthamizh, S., et al., *Silver tungstate nanoparticles: Characterization and Electrochemical Sensing property.* J. ChemTech. Res., 2014. **6**: p. 392-3394.
37. Pinatti, I.M., et al., *Luminescence properties of alpha-Ag2WO4 nanorods co-doped with Li+ and Eu3+ cations and their effects on its structure.* Journal of Luminescence, 2019. **206**: p. 442-454.
38. Jacomaci, N., et al., *Dielectric Behavior of alpha-Ag2WO4 and its Huge Dielectric Loss Tangent.* Materials Research-Ibero-American Journal of Materials, 2019. **22**(4).
39. Neto, N.F.A., et al., *Effect of temperature on the morphology and optical properties of Ag2WO4 obtained by the co-precipitation method: Photocatalytic activity.* Ceramics International, 2019. **45**(12): p. 15205-15212.
40. Li, S.J., et al., *Ag2WO4 nanorods decorated with AgI nanoparticles: Novel and efficient visible-light-driven photocatalysts for the degradation of water pollutants.* Beilstein J. Nanotechnol., 2018. **9**: p. 1308-1316.
41. Rakshitha, R., et al., *Coprecipitation aided synthesis of bimetallic silver tungstate: a response surface simulation of sunlight-driven photocatalytic removal of 2,4-dichlorophenol.* Environ. Sci. Pollut. Res., 2022. **29**: p. 59433-59443.
42. Nubla, K. and N. Sandhyarani, *Ag nanoparticles anchored Ag2WO4 nanorods: An efficient methanol tolerant and durable Pt free electro-catalyst toward oxygen reduction reaction.* Electrochim. Acta, 2020: p. 135942.
43. Pimentel, B., et al., *Antifungal Activity and Biocompatibility of alpha-AgVO3, alpha-Ag2WO4, and beta-Ag2MoO4 Using a Three-Dimensional Coculture Model of the Oral Mucosa.* Front. Bioeng. Biotechnol. , 2022. **10**: p. 14.
44. Foggi, C.C., et al., *Synthesis and evaluation of alpha-Ag2WO4 as novel antifungal agent.* Chem. Phys. Lett., 2017. **674**: p. 125-129.
45. Selvamani, M., et al., *Ag@Ag8W4O16 nanoroasted rice beads with photocatalytic, antibacterial and anticancer activity.* Materials Science & Engineering C-Materials for Biological Applications, 2016. **60**: p. 109-118.
46. Santos, C.J., et al., *Ag2WO4 nanoparticles radiolabeled with technetium-99m: a potential new tool for tumor identification and uptake.* Journal of Radioanalytical and Nuclear Chemistry, 2019.
47. Nobre, F.X., et al., *Antimicrobial properties of α-Ag2WO4 rod-like microcrystals synthesized by sonochemistry and sonochemistry followed by hydrothermal conventional method.* Ultrason. Sonochem., 2019. **58**: p. 104620.

48. van den Berg, A.J. and C.A.H. Juffermans, *The polymorphism of silver tungstate Ag2WO4.* J. Appl. Crystallogr., 1982. **15**(1): p. 114-116.
49. Skarstad, P.M. and S. Geller, *(W4016)8- Polyion in the High Temperature Modification of Silver Tungstate.* Mat. Res. Bull. , 1975. **10**: p. 791-800.
50. Kharade, R.R., et al., *Enhanced electrochromic coloration in Ag nanoparticle decorated WO3 thin films.* Electrochimica Acta, 2013. **102**: p. 358-368.
51. Xiang, Q.J., J.G. Yu, and M. Jaroniec, *Synergetic Effect of MoS2 and Graphene as Cocatalysts for Enhanced Photocatalytic H-2 Production Activity of TiO2 Nanoparticles.* J. Amer. Chem. Soc., 2012. **134**(15): p. 6575-6578.
52. Kako, T., N. Kikugawa, and J. Ye, *Photocatalytic activities of AgSbO3 under visible light irradiation.* Catal. Today, 2008. **131**(1-4): p. 197-202.
53. Lacerda, L.H.d.S., et al., *A diagnosis approach for semiconductor properties evaluation from ab initio calculations: Ag-based materials investigation.* J. Solid State Chem., 2022. **305**: p. 122670.
54. Moura, J.V.B., et al., *Temperature-induced phase transitions in metastable β-Ag2WO4: a Raman scattering study.* Vib. Spectrosc., 2020. **110**: p. 103135.
55. Queisser, H.J. and E.E. Haller, *Defects in Semiconductors: Some Fatal, Some Vital.* Science, 1998. **281**(5379): p. 945-950.
56. Waser, R. and M. Aono, *Nanoionics-based resistive switching memories.* Nature Mater., 2007. **6**(11): p. 833-840.
57. Merkle, R. and J. Maier, *How Is Oxygen Incorporated into Oxides? A Comprehensive Kinetic Study of a Simple Solid-State Reaction with SrTiO3 as a Model Material.* Angew. Chem. Int. Ed., 2008. **47**(21): p. 3874-3894.
58. Alkauskas, A., M.D. McCluskey, and C.G. Van de Walle, *Tutorial: Defects in semiconductors—Combining experiment and theory.* J. Appl. Phys., 2016. **119**(18): p. 181101.
59. Assis, M., et al., *Revealing the Nature of Defects in alpha-Ag2WO4 by Positron Annihilation Lifetime Spectroscopy: A Joint Experimental and Theoretical Study.* Cryst. Growth Des., 2021. **21**(2): p. 1093-1102.
60. Rabes, I. and R. Schenck, *Beiträge zur Chemie der Wolframate.* Z. Anorg. Allg. Chem, 1949. **259**: p. 201–219.
61. Xu, H., et al., *A construction of Ag-modified raspberry-like AgCl/Ag2WO4 with excellent visible-light photocatalytic property and stability.* Mater. Res. Bull., 2018. **102**: p. 342-352.
62. Takahashi, T., S. Ikeda, and O. Yamamoto, *Solid-State Ionics - New High Ionic Conductivity Solid Electrolyte Ag6I4WO4 and Use of this Compound in a Solid-Electrolyte Cell.* J. Electrochem. Soc., 1973. **120**(5): p. 647-651.
63. Bottlebergs, P.H., H. Everts, and G.H.J. Broers, *Phase diagram and high ionic conductivity of the system Na2WO4-Ag2WO4.* Mater. Res. Bull., 1976. **11**: p. 263.
64. Hall, P.G., D.A. Armitage, and R.G. Linford, *Heat capacity of silver tungstate between 80 and 500 K.* J. Chem. Thermodynamics, 1985. **17**: p. 657.
65. Berg, M.A. and A. Jain, *Kinetics and mechanism of reactions of silver tungstate with mercuric bromoiodide and mercuric chlorobromide in the solid state.* Polyhedron, 1992. **11**: p. 2775.

66. Jain, A. and M.A. Berg, *Kinetics and mechanism of solid state reactions of silver tungstate with mercuric bromide and mercuric chloride.* Polyhedron, 1995. **14**: p. 2293.
67. R.P. Raffaelle, et al., *A facile route to thin-film solid state lithium microelectronic batteries.* J. Power Sourc., 2000. **89**: p. 52-55.
68. McKechnie, J.S., et al., *Silver Monotungstates, Ditungstates and Tetratungstates.* J. Inorg. Nucl. Chem., 1979. **41**(2): p. 177-179.
69. Schiraldi, A. and E. Pezzati, *Ag, Cu and Na ionic diffusion in the vitreous superionic conductor Ag6I4WO4.* Z. Phys. Chem. Neue Fol., 1981. **126**(pt2): p. 217-222.
70. Michal, R. and K.E. Saeger, *Metallurgical aspects of silver-based contact materials for air-break switching devices for power engineering.* IEEE Trans. Compon. Hyb. Manufact. Technol., 1989. **12**(1): p. 71-81.
71. Beg, M.A., A. Jain, and K.M. Ghouse, *Studies on silver tungstate-mercuric iodide reaction in solid state.* J. Solid State Chem., 1988. **75**(1): p. 1-6.
72. SIENKO, M.J. and B.R. MAZUMDER, *Some Solid State Studies of Silver-doped WO3.* J. Am. Chem. Soc.,, 1960. **82**: p. 3508.
73. Turkovi, A., et al., *High Temperature Raman Spectroscopy of Silver Tetratungstate, Ag8W4016.* Mat. Res. Bull., 1977. **12**: p. 189-196.
74. Zeng, D.L., H.C. Zhou, and F.G. Su, *Hydrogen-reduction of co-precipitated Ag2WO4/Ag2CO3 mixtures.* Adv. Powder Metall., ed. J.M. Capus and R.M. German. Vol. 1. 1992: Adv. Powder Metall. 193-200.
75. George, T., S. Joseph, and S. Mathew, *Synthesis and characterization of nanophased silver tungstate.* Pramana-J. Phys., 2005. **65**(5): p. 793-799.
76. Qureshi, A.H., S.M. Azhar, and N. Hussain, *The effect of cobalt addition on sintering and microstructural behaviour of silver-tungsten (Ag-W) composite.* J. Therm. Anal. Calorim., 2010. **99**(1): p. 203-209.
77. Wang, B.-Y., et al., *Controllable fabrication of α-Ag2WO4 nanorod-clusters with superior simulated sunlight photocatalytic performance.* Inorganic Chemistry Frontiers, 2019. **6**(1): p. 209-219.
78. Yu, S.H., et al., *General synthesis of single-crystal tungstate nanorods/nanowires: A facile, low-temperature solution approach.* Advanced Functional Materials, 2003. **13**(8): p. 639-647.
79. Wang, P., et al., *Composite Semiconductor H2WO4·H2O/AgCl as an Efficient and Stable Photocatalyst under Visible Light.* Chem. Eur. J., 2008. **14**(34): p. 10543-10546.
80. Bastos, I.S., et al., *Silver tungstate microcrystals and their performance over several clinical multidrug resistant microorganisms.* Colloids Surf. A: Physicochem. Eng. Asp., 2022: p. 129132.
81. Hu, B., et al., *Microwave-assisted synthesis of silver indium tungsten oxide mesocrystals and their selective photocatalytic properties.* Chem. Commun., 2010. **46**(13): p. 2277-2279.
82. Tian, G.R. and S.X. Sun, *Additive induced morphology changes of nano-crystalline SrWO4.* Cryst. Res. Technol., 2011. **46**(4): p. 389-392.

83. Tawde, D., M. Srinivas, and K.V.R. Murthy, *Effect of lead source and cerium (III) doping on structural and photoluminescence properties of PbWO4 microcrystallites synthesized by hydrothermal method.* Phys. Status Solidi A, 2011. **208**(4): p. 803-807.
84. Tian, Y., et al., *Bismuth tungstate nano/microstructures: Controllable morphologies, growth mechanism and photocatalytic properties.* J. Alloys Compd., 2011. **509**(3): p. 724-730.
85. Liu, S.F., I.R. Abothu, and S. Komarneni, *Barium titanate ceramics prepared from conventional and microwave hydrothermal powders.* Mater. Lett., 1999. **38**(5): p. 344-350.
86. Abothu, I.R., et al., *Processing of Pb(Zr0.52Ti0.48)O3 (PZT) ceramics from microwave and conventional hydrothermal powders.* Mater. Res. Bull., 1999. **34**: p. 1411–1419.
87. Somiya, S. and R. Roy, *Hydrothermal synthesis of fine oxide powders.* Bull. Mater. Sci., 2000. **23**: p. 453–460.
88. Godinho, M., et al., *Influence of Microwave Heating on the Growth of Gadolinium-Doped Cerium Oxide Nanorods.* Cryst. Growth Des., 2008. **8**: p. 384–386.
89. Wilson, G.J., et al., *Modification of TiO2 for Enhanced Surface Properties: Finite Ostwald Ripening by a Microwave Hydrothermal Process.* Langmuir, 2006. **22**: p. 2016-2027.
90. Fortuny, M., et al., *Principais aplicações das microondas na produção e refino de petróleo.* Quim. Nova, 2008. **31**: p. 1553.
91. Menezes, R.R., P.M. Souto, and R.H.G.A. Kiminami, *Sinterização de cerâmicas em microondas. Parte I: Aspectos fundamentais.* Cerâmica, 2007. **53**: p. 1.
92. Komarneni, S., R.K. Rajha, and H. Katsuki, *Microwave-hydrothermal processing of titanium dioxide.* Mater. Chem. Phys., 1999. **61**(1): p. 50-54.
93. Wang, X., et al., *Hierarchically porous metastable beta-Ag2WO4 hollow nanospheres: controlled synthesis and high photocatalytic activity.* Nanotechnology, 2013. **24**(16): p. 165602.
94. Zinatloo-Ajabshir, S., et al., *Sonochemical synthesis and characterization of silver tungstate nanostructures as visible-light-driven photocatalyst for waste-water treatment.* Sep. Purif. Technol., 2020. **248**: p. 117062.
95. Ribeiro, L.K., et al. *Tug-of-War Driven by the Structure of Carboxylic Acids: Tuning the Size, Morphology, and Photocatalytic Activity of α-Ag2WO4*. Nanomaterials, 2022. **12**, DOI: 10.3390/nano12193316.
96. Lemos, P.S., et al., *Synthesis and characterization of metastable β-Ag2WO4: an experimental and theoretical approach.* Dalton Trans., 2016. **45**: p. 1185-1191.
97. Ramezani, M., et al., *Silver tungstate nanostructures: electrochemical synthesis and its statistical optimization.* J. Mater. Sci.-Mater. El., 2015. **26**(6): p. 3861-3867.
98. Li, J., et al., *Facile formation of Ag2WO4/AgX (X= Cl, Br, I) hybrid nanorods with enhanced visible-light-driven photoelectrochemical properties.* Mater. Res. Bull., 2015. **61**: p. 315-320.
99. Gupta, S.K., et al., *Doping-Induced Room Temperature Stabilization of Metastable β-Ag2WO4 and Origin of Visible Emission in α- and β-Ag2WO4: Low Temperature Photoluminescence Studies.* J. Phys. Chem. C, 2016. **120**(13): p. 7265-7276.

100. Liu, D.Q., et al., *Experimental and theoretical investigation on photocatalytic activities of 1D Ag/Ag2WO4 nanostructures.* Nanotechnology, 2017. **28**(38).
101. Alvarez-Roca, R., et al., *Selective Synthesis of α-, β-, and γ-Ag2WO4 Polymorphs: Promising Platforms for Photocatalytic and Antibacterial Materials.* Inorg. Chem., 2021. **60**(2): p. 1062-1079.
102. Sreedevi, A., et al., *Chemical synthesis, structural characterization and optical properties of nanophase α-Ag2WO4.* Indian J. Phys., 2015. **89**(9): p. 889-897.
103. Sreedevi, A., et al., *Synthesis and characterization of silver tungstate/iron phthalocyanine nanocomposite for electronic applications.* Eur. Phys. J. B, 2017. **90**(6).
104. Sreedevi, A., et al., *Silver Tungstate Nanoparticles for the Detection of Ethanol, Ammonia and Acetone Gases.* Journal of Electronic Materials, 2018. **47**(10): p. 6328-6333.
105. Peng, Z.A. and X. Peng, *Nearly Monodisperse and Shape-Controlled CdSe Nanocrystals via Alternative Routes: Nucleation and Growth.* J. Am. Chem. Soc., 2002. **124**(13): p. 3343-3353.
106. Mullin, J.W., *Crystallization*. 3rd ed. 1997, Oxford: Butterworth-Heinemann.
107. Ng, C.H.B. and W.Y. Fan, *Preparation of highly uniform 1-dimensional alpha-Ag2WO4 nanostructures with controllable aspect ratio and study of the growth mechanism.* Crystengcomm, 2016. **18**(41): p. 8010-8019.
108. Andrés, J., et al., *Effects of surface stability on the morphological transformation of metals and metal oxides as investigated by first-principles calculations.* Nanotechnology 2015. **26**(40): p. 405703-405713.
109. Macedo, N.G., et al., *Surfactant-Mediated Morphology and Photocatalytic Activity of α-Ag2WO4 Material.* J. Phys. Chem. C, 2018. **122**(15): p. 8667-8679.
110. Macedo, N.G., et al., *Tailoring the Bactericidal Activity of Ag Nanoparticles/α-Ag2WO4 Composite Induced by Electron Beam and Femtosecond Laser Irradiation: Integration of Experiment and Computational Modeling.* ACS Appl. Bio Mater., 2019. **2**(2): p. 824-837.
111. de Abreu, C.B., et al., *Toxicity of alpha-Ag2WO4 microcrystals to freshwater microalga Raphidocelis subcapitata at cellular and population levels.* Chemosphere, 2022. **288**.
112. de Abreu, C.B., et al., *Effects of alpha-Ag2WO4 crystals on photosynthetic efficiency and biomolecule composition of the algae Raphidocelis subcapitata.* Wat. Air Soil Poll., 2022. **233**(4): p. 11.
113. Sczancoski, J.C., et al., *Atomic Diffusion Induced by Electron-Beam Irradiation: An in Situ Study of Ag Structures Grown from alpha-Ag2WO4.* Cryst. Growth Des., 2019. **19**(1): p. 106-115.
114. Cruz, L., et al., *Multi-dimensional architecture of Ag/alpha-Ag2WO4 crystals: insights into microstructural, morphological, and photoluminescence properties.* CrystEngComm, 2020. **22**(45): p. 7903-7917.
115. Laier, L.O., et al., *Surface-dependent properties of alpha-Ag2WO4: a joint experimental and theoretical investigation.* Theor. Chem. Acc., 2020. **139**(7): p. 108.

116. Roca, R.A., et al., *Uncovering the metastable gamma-Ag2WO4 phase: a joint experimental and theoretical study.* RSC Adv., 2017. **7**(10): p. 5610-5620.
117. Neto, N.F.A., et al., *Stabilization of the gamma-Ag2WO4 metastable pure phase by coprecipitation method using polyvinylpyrrolidone as surfactant: Photocatalytic property.* Ceram. Int., 2020. **46**(10): p. 14864-14871.
118. Pereira, P.F.S., et al., *Inactivation of SARS-CoV-2 by a chitosan/α-Ag2WO4 composite generated by femtosecond laser irradiation.* Sci. Rep., 2022. **12**(1): p. 8118.
119. Ferrer, M.M., et al., *A 3D platform for the morphology modulation of materials: First principles calculations on the thermodynamic stability and surface structure of metal oxides: Co3O4, α-Fe2O3, and In2O3.* Modell. Simul. Mater. Sci. Eng., 2016. **24**: p. 025007-025016.
120. Gouveia, A.F., et al., *Modeling the atomic-scale structure, stability, and morphological transformations in the tetragonal phase of LaVO4.* Chem. Phys. Lett., 2016. **660**: p. 87-92.
121. Gouveia, A.F., et al., *Reading at exposed surfaces: theoretical insights into photocatalytic activity of ZnWO4.* Front. Res. Today, 2018. **1**.
122. Ribeiro, R.A.P., et al., *Connecting the surface structure, morphology and photocatalytic activity of Ag2O: An in depth and unified theoretical investigation.* Appl. Surf. Sci., 2020. **509**: p. 145321.
123. Ribeiro, R.A.P., et al., *First principle investigation of the exposed surfaces and morphology of beta-ZnMoO4.* J. Appl. Phys., 2019. **126**(23).
124. Oliveira, M.C., et al., *Geometry, electronic structure, morphology, and photoluminescence emissions of BaW1-xMoxO4 (x=0, 0.25, 0.50, 0.75, and 1) solid solutions: Theory and experiment in concert.* Appl. Surf. Sci., 2019. **463**: p. 907-917.
125. Oliveira, F.K.F., et al., *Experimental and theoretical study to explain the morphology of CaMoO4 crystals.* J. Phys. Chem. Solids, 2018. **114**: p. 141-152.
126. Lipsky, F., et al., *Unraveling the relationship between exposed surfaces and the photocatalytic activity of Ag3PO4: an in-depth theoretical investigation.* RSC Adv., 2020. **10**: p. 30640-30649.
127. Wulff, G., *On the question of speed of growth and dissolution of crystal surfaces.* Z. Kristallogr., 1901. **34**(5/6): p. 449-530.
128. Guo, J., et al., *Stability of eutectic carbide in Fe-Cr-Mo-W-V-C alloy by first-principles calculation.* Mater. Des., 2016. **106**: p. 355-362.
129. Meng, J., et al., *Cubic-like BaZrO3 nanocrystals with exposed {001}/{011} facets and tuned electronic band structure for enhanced photocatalytic hydrogen production.* J. Mater. Sci., 2019. **54**(3): p. 1967-1976.
130. Habibzadeh Mashatooki, M., et al., *Investigation of TiO2 anatase (1 0 1), (1 0 0) and (1 1 0) facets as immobilizer for a potential anticancer RNA aptamer: a classical molecular dynamics simulation.* Mol. Simul., 2019. **45**(11): p. 849-858.
131. Wen, Y. and D. Xia, *A thermodynamics model for morphology prediction of aluminum nano crystals fabricated by the inert gas condensation method.* Nanotechnology, 2018. **29**(12): p. 125301.

132. Paz, C.V., et al., *Evaluation of surface phenomena involved in photocatalytic degradation of Acid Blue 9 by TiO2 catalysts of single and mixed phase – A theoretical and experimental study.* Appl. Surf. Sci., 2020. **508**: p. 145114.
133. Habibzadeh Mashatooki, M., A. Abbasi, and J. Jahanbin Sardroodi, *In silico studies of the interaction of the colon cancer receptor and RNA aptamer adsorbed on (1 0 1) facet of TiO2 nanoparticle investigated by molecular dynamics simulation.* Adsorption, 2020. **26**(6): p. 941-954.
134. Sivakumar, A., et al., *Comparative Assessment of Crystallographic Phase Stability of Anatase and Rutile TiO2 at Dynamic Shock Wave Loaded Conditions.* J. Inorg. Organomet. Polym. Mater., 2022. **32**(3): p. 967-972.
135. Tang, M., et al., *First principles study of electronic structure of cerium carbonate unit cell to explain its crystal morphology.* Emerg. Mater., 2022.
136. Kakil, S.A., H.Y. Abdullah, and T.G. Abdullah, *Electronic properties of (TiO2)33 nanocrystals with nitrogen impurities at different facets: a DFT study.* Mol. Simul., 2021. **47**(14): p. 1185-1197.
137. Xing, C., et al., *The role of ligands in pressure-induced phase transition of gold nanoribbons.* Ph. Transit., 2021. **94**(3-4): p. 123-133.
138. Bair, J.L., N.S. Deshmukh, and D.G. Abrecht, *Spherical Gaussians: An intuitive method for creating complex anisotropies in interface energies for the phase field method.* Comput. Mater. Sci., 2021. **188**: p. 110126.
139. Gouveia, A.F., et al., *Modulating the properties of multifunctional semiconductors by means of morphology: Theory meets experiments.* Comput. Mater. Sci., 2021. **188**: p. 110217.
140. Pinatti, I.M., et al., *Low temperature micro Raman and laser induced upconversion and downconversion spectra of europium doped silver tungstate Ag2-3xEuxWO4 nanorods.* Journal of Materials Science-Materials in Electronics, 2017. **28**(10): p. 7029-7035.
141. Stearns, E.I., *Commission Internationale de L'Éclairage, Colorimetry, 2nd ed., Publication CIE No. 15.2, 78 + vi pp., paperbound, price $28; Central Bureau of the CIE, Vienna, 1987. Available in the U.S. from the U.S. National Committee, CIE, c/o National Bureau of Stan.* Color Research & Application, 1988. **13**: p. 64-65.
142. Pinatti, I.M., et al., *Rare earth doped silver tungstate for photoluminescent applications.* Journal of Alloys and Compounds, 2019. **771**: p. 433-447.
143. Wang, J., et al., *Morphology modification, spectrum, and optical thermometer application of rare earth ions doped ?-Ag 2 WO 4.* J. Lumin., 2020. **224**.
144. Huangfu, Z.B., et al., *Comparative analysis of the emission of Eu3+ doped in alpha- and beta-Ag2WO4.* J. Mol. Struct. , 2022. **1269**: p. 6.
145. Ayappan, C., et al., *Copper ions induced alpha-Ag2-2xCuxWO4 (0 <= x <= 0.12) solid solutions with favorable sunlight photocatalytic removal of toxic pollutants.* J. Alloys Compd., 2021. **871**.
146. do Nascimento, M.V.B., et al., *Ag2-xCuxWO4 Solid Solution: Structure, Morphology, Optical Properties, and Photocatalytic Performance in the Degradation of RhB under Blue Light-Emitting Device Irradiation.* J. Phys. Chem. C, 2021. **125**(22): p. 11875-11890.

147. Penha, M.D., et al., *Structure, optical properties, and photocatalytic activity of α-Ag2W0.75Mo0.25O4.* Mater. Res. Bull., 2020. **132**: p. 111011.
148. Pereira, P.F.S., et al., *alpha-Ag2-2xZnxWO4 (0 </= x </= 0.25) Solid Solutions: Structure, Morphology, and Optical Properties.* Inorg. Chem., 2017. **56**(13): p. 7360-7372.
149. Pereira, W.d.S., et al., *Effects of chemical substitution on the structural and optical properties of α-Ag2−2xNixWO4 (0 ≤ x ≤ 0.08) solid solutions.* Phys. Chem. Chem. Phys., 2016. **18**(31): p. 21966-21975.
150. Pereira, P.F., et al. *Disclosing the Biocide Activity of alpha-Ag2-2xCuxWO4 (0 ≤ x ≤ 0.16) Solid Solutions*. Int. J. Mol. Sci., 2022. **23**, DOI: 10.3390/ijms231810589.
151. Marzieh, S., S. Ehsan, and Z. Mostafa, *Fabrication, characterization, antibacterial properties, and the possibility of introducing silver tungstate nanoparticles with Zn as photosensitizers for photodynamic therapy.* Appl. Phys. A: Mater. Sci. Process. , 2022. **128**(9): p. 10.
152. Li, Y.F., et al., *In situ loading of Ag2WO4 on ultrathin g-C3N4 nanosheets with highly enhanced photocatalytic performance.* J. Hazard. Mater., 2016. **313**: p. 219-228.
153. Li, Y., et al., *Efficient water disinfection with Ag2WO4-doped mesoporous g-C3N4 under visible light.* J. Hazard. Mater., 2017. **338**: p. 33-46.
154. Zhu, B.C., et al., *Fabrication and photocatalytic activity enhanced mechanism of direct Z-scheme g-C3N4/Ag2WO4 photocatalyst.* Appl. Surf. Sci., 2017. **391**: p. 175-183.
155. Zhu, Z.Y., F. Zhou, and S. Zhan, *Enhanced antifouling property of fluorocarbon resin coating (PEVE) by the modification of g-C3N4/Ag2WO4 composite step-scheme photocatalyst.* Appl. Surf. Sci., 2020. **506**.
156. Huang, J.X., et al., *Ultrathin Ag2WO4-coated P-doped g-C3N4 nanosheets with remarkable photocatalytic performance for indomethacin degradation.* J. Hazard. Mater., 2020. **392**.
157. Vignesh, K. and M. Kang, *Facile synthesis, characterization and recyclable photocatalytic activity of Ag2WO4@g-C3N4.* Mater. Sci. Eng. B: Adv. Funct. Solid-State Mater. , 2015. **199**: p. 30-36.
158. Dai, K., et al., *A facile fabrication of plasmonic g-C3N4/Ag2WO4/Ag ternary heterojunction visible-light photocatalyst.* Mater. Chem. Phys., 2016. **177**: p. 529-537.
159. Jiang, X.L., et al., *Preparation and Photocatalytic Activity of an Inorganic-Organic Hybrid Photocatalyst Ag2WO4/g-C3N4.* J. Inorg. Organomet. Polym. Mater., 2017. **27**(6): p. 1683-1693.
160. Wang, Y., et al., *AgBr and GO co-decorated g-C3N4/Ag2WO4 composite for enhanced photocatalytic activity of contaminants degradation.* J. Photochem. Photobiol. A: Chem., 2019. **382**: p. 111957.
161. Alosaimi, E.H., et al., *Investigation of Fe-Doped Graphitic Carbon Nitride-Silver Tungstate as a Ternary Visible Light Active Photocatalyst.* J. Chem., 2021. **2021**: p. 18.
162. Vinoth, S., M. Govindasamy, and S.F. Wang, *Solvothermal synthesis of silver tungstate integrated with carbon nitrides matrix composites for highly sensitive*

electrochemical nitrofuran derivative sensing in biological samples. Anal. Chim. Acta, 2022. **1192**: p. 11.
163. Wu, G.Y. and W.N. Xing, *Facile and fabrication of semiconductor silver tungstate loaded on the graphene oxide surface and its effective enhanced catalytic performance.* Fresenius Environ. Bull., 2019. **28**(3): p. 2012-2021.
164. Wu, G.Y. and W.N. Xing, *Fabrication of ternary visible-light-driven semiconductor photocatalyst and its effective photocatalytic performance.* Materials Technology, 2019. **34**(5): p. 292-300.
165. Fang, Y., Y. Cao, and Q.L. Chen, *Synthesis of an Ag2WO4/Ti3C2 Schottky composite by electrostatic traction and its photocatalytic activity.* Ceram. Int., 2019. **45**(17): p. 22298-22307.
166. Adib, K., et al., *Sonochemical synthesis of Ag2WO4/RGO-based nanocomposite as a potential material for supercapacitors electrodes.* Ceram. Int., 2021. **47**(10): p. 14075-14086.
167. Wu, X.F., et al., *Designing visible-light-driven direct Z-scheme Ag2WO4/WS2 heterojunction to enhance photocatalytic activity.* J. Mater. Sci.: Mater. Electron., 2018. **29**(17): p. 14874-14882.
168. Akshatha, G., et al., *Hybrid Nano-Composites by Deposition of Ag2WO4/Carbon Nanotube: Efficient Biological Application.* J. Environ. Toxicol., 2021. **7**(1): p. 1035.
169. He, H.B., et al., *Synthesis and characterization of robust Ag2S/Ag2WO4 composite microrods with enhanced photocatalytic performance.* J. Mater. Res., 2016. **31**(17): p. 2598-2607.
170. He, H.B., et al., *Sonochemical fabrication, characterization and enhanced photocatalytic performance of Ag2S/Ag2WO4 composite microrods.* Chin. J. Catal., 2016. **37**(11): p. 1841-1850.
171. Ayappan, C., et al., *Facile preparation of novel Sb2S3 nanoparticles/rod-like alpha-Ag2WO4 heterojunction photocatalysts: Continuous modulation of band structure towards the efficient removal of organic contaminants.* Sep. Purif. Technol., 2020. **236**.
172. Thangavel, S., et al., *Efficient visible-light photocatalytic and enhanced photocorrosion inhibition of Ag2WO4 decorated MoS2 nanosheets.* J. Phy. Chem. Solids, 2017. **110**: p. 266-273.
173. Kokilavani, S., et al., *Integrating Ag2WO4 on VS4 nanoplates with synergy of plasmonic photocatalysis and boosted visible-light harvesting and its antibacterial applications.* J. Alloys Compd., 2021. **865**.
174. Kokilavani, S., et al., *Enhanced visible light driven photocatalytic and antibacterial activities of Ag2WO4 decorated ZnS nanocomposite.* Ceram. Int., 2021. **47**(9): p. 12997-13006.
175. Kokilavani, S., et al., *Preparation of plasmonic CoS/Ag2WO4 nanocomposites: Efficient visible light driven photocatalysts and enhanced anti-microbial activity.* Colloid Interface Sci. Commun., 2021. **42**.
176. Kokilavani, S., et al., *Decoration of Ag2WO4 on plate-like MnS for mitigating the charge recombination and tuned bandgap for enhanced white light photocatalysis and antibacterial applications.* J. Alloys Compd., 2022. **889**: p. 161662.

177. Wang, P., et al., *Ag@AgCl: A highly efficient and stable photocatalyst active under visible light.* Angew. Chem. Int. Ed., 2008. **47**(41): p. 7931-7933.
178. Kuai, L., et al., *Facile Subsequently Light-Induced Route to Highly Efficient and Stable Sunlight-Driven Ag-AgBr Plasmonic Photocatalyst.* Langmuir, 2010. **26**(24): p. 18723-18727.
179. Amirjani, A. and D.F. Haghshenas, *Ag nanostructures as the surface plasmon resonance (SPR)-based sensors: A mechanistic study with an emphasis on heavy metallic ions detection.* Sens. Actuators B Chem., 2018. **273**: p. 1768-1779.
180. He, H., et al., *Surface decoration of microdisk-like g-C3N4/diatomite with Ag/AgCl nanoparticles for application in Cr(VI) reduction.* Sustain. Mater. Technol., 2019. **22**: p. e00127.
181. Wang, X.F., et al., *In situ anion-exchange synthesis and photocatalytic activity of Ag8W4O16/AgCl-nanoparticle core-shell nanorods.* J. Mol. Catal. A Chem., 2011. **334**(1-2): p. 52-59.
182. Lu, Y., et al., *Preparation and characterisations of silver halide/silver tungstate heterocrystals with enhanced photocatalytic properties.* Mater. Technol., 2017. **32**(3): p. 178-185.
183. Li, S.J., et al., *Construction of a novel ternary Ag/AgBr/Ag2WO4 composite for efficient photocatalytic removal of Rhodamine B dye and tetracycline hydrochloride antibiotic.* Mater. Lett., 2018. **224**: p. 29-32.
184. Zhang, L.L., et al., *Accelerated degradation of pollutants via a close interface connection in heterojunction, and special solid-liquid interactions.* J. Colloid Interface Sci., 2019. **553**: p. 598-605.
185. Yin, H.F., et al., *Surfactant-assisted synthesis of direct Z-scheme AgBr/beta-Ag2WO4 heterostructures with enhanced visible-light-driven photocatalytic activities.* Mater. Sci. Semicond. Process., 2020. **105**.
186. Salesi, S. and A. Nezamzadeh-Ejhieh, *Boosted photocatalytic effect of binary AgI/Ag2WO4 nanocatalyst: characterization and kinetics study towards ceftriaxone photodegradation.* Environ. Sci. Pollut. Res., 2022.
187. Zhang, S.H., et al., *Highly effective photoelectrochemical performance of solar energy materials based on Ag2WO4-AgX (X = Cl, Br, I) sensitized TiO2 nanotube arrays.* Ceram. Int., 2018. **44**(6): p. 6659-6665.
188. Feizpoor, S. and A. Habibi-Yangjeh, *Integration of Ag2WO4 and AgBr with TiO2 to fabricate ternary nanocomposites: Novel plasmonic photocatalysts with remarkable activity under visible light.* Mater. Res. Bull., 2018. **99**: p. 93-102.
189. Pirhashemi, M. and A. Habibi-Yangjeh, *Preparation of novel nanocomposites by deposition of Ag2WO4 and AgI over ZnO particles: Efficient plasmonic visible-light-driven photocatalysts through a cascade mechanism.* Ceram. Int., 2017. **43**(16): p. 13447-13460.
190. Hemmati-Eslamlu, P., et al., *Ultrasonic-assisted decoration of Ag2WO4, AgI, and Ag nanoparticles over tubular g-C3N4: Plasmonic photocatalysts for impressive removal of tetracycline under visible light.* Photochem. Photobiol. Sci. , 2022. **21**(7): p. 1201-1215.

191. Rajamohan, S., et al., *Fe3O4-Ag2WO4: facile synthesis, characterization and visible light assisted photocatalytic activity.* New J. Chem., 2017. **41**(20): p. 11722-11730.
192. Ghobadifard, M. and S. Mohebbi, *Novel nanomagnetic Ag/beta-Ag2WO4/CoFe2O4 as a highly efficient photocatalyst under visible light irradiation.* New J. Chem., 2018. **42**(12): p. 9530-9542.
193. Shen, J., et al., *Design and preparation of easily recycled Ag2WO4@ZnO@Fe3O4 ternary nanocomposites and their highly efficient degradation of antibiotics.* J. Mater. Sci., 2016. **51**(16): p. 7793-7802.
194. Jabbar, Z.H., S.E. Ebrahim, and S.H. Ammar, *Supported heterogeneous nanocomposites (SiO2/Fe3O4/Ag2WO4) for visible-light-driven photocatalytic disinfection against E. coli.* Mater. Sci. Semicond. Process., 2022. **141**: p. 106427.
195. Mousavi, M. and A. Habibi-Yangjeh, *Magnetically recoverable highly efficient visible-light-active g-C3N4/Fe3O4/Ag2WO4/AgBr nanocomposites for photocatalytic degradations of environmental pollutants.* Adv. Powder Technol., 2018. **29**(1): p. 94-105.
196. Jabbar, Z.H. and S.E. Ebrahim, *Synthesis, characterization, and photocatalytic degradation activity of core/shell magnetic nanocomposites (Fe3O4@SiO2@Ag2WO4@Ag2S) under visible light irradiation.* Opt. Mater. , 2021. **122**: p. 12.
197. Qiu, F.X., et al., *Fabrication of a novel hierarchical flower-like hollow structure Ag2WO4/WO3 photocatalyst and its enhanced visible-light photocatalytic activity.* Powder Technol., 2017. **317**: p. 287-292.
198. Zou, X.J., et al., *Facile anion exchange to construct uniform AgX (X = Cl, Br, I)/Ag2CrO4 NR hybrids for efficient visible light driven photocatalytic activity.* Solar Energy, 2018. **169**: p. 392-400.
199. Wang, Y., et al., *Z-type electronic structure and enhanced photocatalytic performance of silver tungstate - phosphorus and aluminum co-doped zinc oxide heterogeneous catalysts.* Mater. Technol., 2017. **32**(9): p. 523-534.
200. Pirhashemi, M. and A. Habibi-Yangjeh, *Ultrasonic-assisted preparation of plasmonic ZnO/Ag/Ag2WO4 nanocomposites with high visible-light photocatalytic performance for degradation of organic pollutants.* J. Colloid Interface Sci., 2017. **491**: p. 216-229.
201. Shawky, A., et al., *One-pot synthesis of Mn3O4-coupled Ag2WO4 nanocomposite photocatalyst for enhanced photooxidative desulfurization of thiophene under visible light irradiation.* Appl. Nanosci., 2020. **10**(5): p. 1545-1554.
202. Cui, Y., et al., *Boosting photoelectrochemical and photocatalytic performances of electronspun WO3 nanofibers by combining with biphase-Ag2WO4.* Mater. Sci. Semicon. Proc., 2020. **120**.
203. Mohamed, M.M. and H. El-Farsy, *Rapid reduction of nitroarenes photocatalyzed by an innovative Mn3O4/alpha-Ag2WO4 nanoparticles.* Sci. Rep., 2020. **10**(1).
204. Zhou, L., et al., *Preparation of novel 0D/2D A(g2)WO(4)/WO3 Step-scheme heterojunction with effective interfacial charges transfer for photocatalytic contaminants degradation and mechanism insight.* Chem. Eng. J., 2021. **420**.

205. Liu, X., Y. Kang, and Y. Wang, *Novel high-efficiency visible-light-driven p-n heterojunction β-Bi2O3/Ag2WO4 photocatalysts.* Chem. Phys. Lett., 2022. **790**: p. 139347.
206. Balasurya, S., et al., *Photodegradation of 5-flurouracil, carvedilol, para-chlorophenol and methimazole with 3D MnWO4 nanoflower modified Ag2WO4 nanorods: A non-genotoxic nanomaterial for water treatment.* Chemosphere, 2022. **297**: p. 10.
207. Wang, F.X., et al., *Flower-like Ag2WO4/CeO2 heterojunctions with oxygen vacancies and expedited charge carrier separation boost the photocatalytic degradation of dyes and drugs.* Dalton Trans., 2022. **51**(26): p. 10179-10185.
208. Trench, A.B., et al., *Interface matters: Design of an efficient alpha-Ag2WO4/Ag3PO4 photocatalyst.* Mater. Chem. Phys. , 2022. **280**: p. 12.
209. Farsi, M. and A. Nezamzadeh-Ejhieh, *A Z-scheme Cobalt(II) oxide-silver tungstate nano photocatalyst: Experimental design and mechanism study for the degradation of methylene blue.* Surf. Interfaces 2022. **32**: p. 16.
210. Farsi, M. and A. Nezamzadeh-Ejhieh, *A coupled Cobalt(II) oxide-Silver Tungstate nano-photocatalyst: Moderate characterization and evaluation of the photocatalysis kinetics towards methylene blue in aqueous solution.* Polyhedron, 2022. **219**: p. 12.
211. Wang, Y., Y. Kang, and X.H. Liu, *Construction of visible-light-driven ZnBi2O4/Ag2WO4 p-n heterojunction for restraining carrier recombination and improving visible-light photocatalytic performance.* J. Mater. Sci. Mater. Electron. , 2022. **33**(25): p. 19827-19838.
212. Mondego, M., et al., *Blue and red light photoluminescence emission at room temperature from CaTiO3 decorated with alpha-Ag2WO4.* Ceram. Int., 2017. **43**(7): p. 5759-5766.
213. Ayappan, C., et al., *One-step hydrothermal synthesis of CaWO4/alpha-Ag2WO4 heterojunction: An efficient photocatalyst for removal of organic contaminants.* Mater. Sci. Semicon. Proc., 2019. **104**.
214. Li, T.F., et al., *Mechanisms for Highly Efficient Mineralization of Bisphenol A by Heterostructured Ag2WO4/Ag3PO4 under Simulated Solar Light.* ACS Sustain. Chem. Eng., 2019. **7**(4): p. 4177-4185.
215. Askari, P., S. Mohebbi, and T.O. Do, *High performance plasmonic activation of Ag on beta-Ag2WO4/BiVO4 as nanophotocatalyst for oxidation of alcohols by incident visible light.* J. Photochem. Photobiol. A, 2018. **367**: p. 56-65.
216. Lv, J.L., et al., *In situ controllable synthesis of novel surface plasmon resonance-enhanced Ag2WO4/Ag/Bi2MoO6 composite for enhanced and stable visible light photocatalyst.* Appl. Surf. Sci., 2017. **391**: p. 507-515.
217. Rafiq, U. and K. Majid, *Mitigating the charge recombination by the targeted synthesis of Ag2WO4/Bi2Fe4O9 composite: The facile union of orthorhombic semiconductors towards efficient photocatalysis.* J. Alloys Compd., 2020. **842**.
218. Chinnathambi, A., et al., *Performance analysis of novel La6WO12/Ag2WO4 nano-system for efficient visible-light photocatalysis and antimicrobial activity.* J. Alloys Compd., 2021. **879**.

219. Rafiq, U., et al., *Solvothermal synthesis of Ag2WO4/Sb2WO6 heterostructures for enhanced charge transfer properties and efficient visible-light-driven photocatalytic activity and stability.* J. Environ. Chem. Eng., 2020. **8**(5).
220. Elgorban, A.M., A.A. Al Kheraif, and A. Syed, *Construction of Ag2WO4 decorated CoWO4 nano-heterojunction with recombination delay for enhanced visible light photocatalytic performance and its antibacterial applications.* Colloids Surf. A Physicochem. Eng. Asp., 2021. **629**.
221. Emam, H.E., et al., *Doping of silver vanadate and silver tungstate nanoparticles for enhancement the photocatalytic activity of MIL-125-NH2 in dye degradation.* J. Photochem. Photobiol. A, 2019. **383**.
222. Sofi, F.A. and K. Majid, *Plasmon induced interfacial charge transfer across Zr-based metal-organic framework coupled Ag2WO4 heterojunction functionalized by Ag NPs: Efficient visible light photocatalyst.* Chem. Phys. Lett., 2019. **720**: p. 7-14.
223. Sreedevi, A., et al., *Structural and optical modifications of the Ag2WO4/CoPc nanocomposite for potential applications.* Eur. Phys. J. Plus, 2016. **131**(1): p. 1-8.
224. Wang, H., et al., *Study on Ag2WO4/g-C3N4 Nanotubes as an Efficient Photocatalyst for Degradation of Rhodamine B.* J. Inorg. Organomet. Polym. Mater., 2020. **30**(12): p. 4847-4857.
225. Wang, Z., et al., *Advances in designing heterojunction photocatalytic materials.* Chinese J. Catal., 2021. **42**(5): p. 710-730.
226. Xie, L., et al., *Recent advances on heterojunction-based photocatalysts for the degradation of persistent organic pollutants.* Chem. Eng. J., 2021. **426**: p. 130617.
227. Ni, Z., et al., *Facile construction of 3D hierarchical flower-like Ag2WO4/Bi2WO6 Z-scheme heterojunction photocatalyst with enhanced visible light photocatalytic activity.* Appl. Surf. Sci., 2022. **576**: p. 151868.
228. Cen, S., et al., *Direct Z-scheme Ag2WO4/BiOCl composite photocatalyst for efficient photocatalytic degradations of dissolved organic impurities.* Optik, 2021. **243**: p. 166847.
229. Sun, Y., et al., *Efficient removal of lomefloxacin by Z-scheme MrGO/Ag2WO4 heterojunction recyclable composite under visible light: Mechanism of adsorption and photodegradation.* J. Environ. Chem. Eng. , 2022. **10**(1): p. 12.
230. Zhai, X.-Y., et al., *In situ construction of a direct Z-scheme AgBr/α-Ag2WO4 heterojunction with promoted spatial charge migration and photocatalytic performance.* New J. Chem., 2021. **45**(6): p. 3128-3137.
231. Kim, J.-U., et al., *Synthesis of Gold Nanoparticles from Gold(I)−Alkanethiolate Complexes with Supramolecular Structures through Electron Beam Irradiation in TEM.* Journal of the American Chemical Society, 2005. **127**(28): p. 9962-9963.
232. Wang, P.-I., et al., *Novel growth mechanism of single crystalline Cu nanorods by electron beam irradiation.* Nanotechnology, 2003. **15**(1): p. 218-222.
233. Yen, M.-Y., et al., *Convergent Electron Beam Induced Growth of Copper Nanostructures: Evidence of the Importance of a Soft Template.* Langmuir, 2004. **20**(2): p. 279-281.
234. Ghatak, J., W. Guan, and G. Möbus, *In situ TEM observation of lithium nanoparticle growth and morphological cycling.* Nanoscale, 2012. **4**(5): p. 1754-1759.

235. Gnanavel, T. and G. Möbus, *In-situ cobalt nanocrystal synthesis by intense electron beams in TEM.* J. Phys.: Conf. Ser., 2012. **371**(1): p. 012047.
236. Assis, M., et al., *Laser-induced formation of bismuth nanoparticles.* Phys. Chem. Chem. Phys., 2018. **20**(20): p. 13693-13696.
237. Andres, J., et al., *A Combined Experimental and Theoretical Study on the Formation of Ag Filaments on beta-Ag2MoO4 Induced by Electron Irradiation.* Part. Part. Syst. Char., 2015. **32**(6): p. 646-651.
238. Botelho, G., et al., *Experimental and Theoretical Study on the Structure, Optical Properties, and Growth of Metallic Silver Nanostructures in Ag3PO4.* J. Phys. Chem. C, 2015. **119**: p. 6293-6306.
239. de Oliveira, R.C., et al., *An Experimental and Computational Study of beta-AgVO3: Optical Properties and Formation of Ag Nanoparticles.* J. Phys. Chem. C, 2016. **120**(22): p. 12254-12264.
240. Fabbro, M.T., et al., *Understanding the formation and growth of Ag nanoparticles on silver chromate induced by electron irradiation in electron microscope: A combined experimental and theoretical study.* J. Solid State Chem., 2016. **239**: p. 220-227.
241. Costa, J.P.d.C.d., et al., *Electron beam irradiation for the formation of thick Ag film on Ag3PO4.* RSC Adv., 2020. **10**(37): p. 21745-21753.
242. Kamino, T., et al., *Development of a Multifunctional Specimen Heating Holder and its Application.* Microscopy and Microanalysis, 2007. **13**(S02): p. 976-977.
243. Nam, S.W., et al., *Electrical Wind Force-Driven and Dislocation-Templated Amorphization in Phase-Change Nanowires.* Science, 2012. **336**(6088): p. 1561-1566.
244. Parent, L.R., et al., *Direct in Situ Observation of Nanoparticle Synthesis in a Liquid Crystal Surfactant Template.* ACS Nano, 2012. **6**(4): p. 3589-3596.
245. Saka, H., et al., *In situ heating transmission electron microscopy.* MRS Bull., 2008. **33**(2): p. 93-100.
246. Yaguchi, T., et al., *Development of a technique for in situ high temperature TEM observation of catalysts in a highly moisturized air atmosphere.* J. Electron Microsc., 2012. **61**(4): p. 199-206.
247. Lin, P.A., et al., *Shape-Controlled Au Particles for InAs Nanowire Growth.* Nano Lett., 2012. **12**(1): p. 315-320.
248. Rudolph, D., et al., *Direct Observation of a Noncatalytic Growth Regime for GaAs Nanowires.* Nano Lett., 2011. **11**(9): p. 3848-3854.
249. Evans, J.E., et al., *Controlled Growth of Nanoparticles from Solution with In Situ Liquid Transmission Electron Microscopy.* Nano Lett., 2011. **11**(7): p. 2809-2813.
250. Radisic, A., F.M. Ross, and P.C. Searson, *In situ study of the growth kinetics of individual island electrodeposition of copper.* J. Phys. Chem. B, 2006. **110**(15): p. 7862-7868.
251. Williamson, M.J., et al., *Dynamic microscopy of nanoscale cluster growth at the solid-liquid interface.* Nat. Mater., 2003. **2**(8): p. 532-536.
252. Ribeiro, C., et al., *In situ oriented crystal growth in a ceramic nanostructured system.* J. Appl. Phys., 2005. **97**(2).

253. Yang, Y.C., et al., *Observation of conducting filament growth in nanoscale resistive memories.* Nature Commun., 2012. **3**.
254. Huang, J.Y., et al., *In situ observation of graphene sublimation and multi-layer edge reconstructions.* Proceedings of the National Academy of Sciences of the United States of America, 2009. **106**(25): p. 10103-10108.
255. Yuk, J.M., et al., *High-Resolution EM of Colloidal Nanocrystal Growth Using Graphene Liquid Cells.* Science, 2012. **336**(6077): p. 61-64.
256. Park, J., et al., *Direct Observation of Nanoparticle Superlattice Formation by Using Liquid Cell Transmission Electron Microscopy.* ACS Nano, 2012. **6**(3): p. 2078-2085.
257. Xin, H.L.L. and H.M. Zheng, *In Situ Observation of Oscillatory Growth of Bismuth Nanoparticles.* Nano Lett., 2012. **12**(3): p. 1470-1474.
258. Dayeh, S.A. and S.T. Picraux, *Direct Observation of Nanoscale Size Effects in Ge Semiconductor Nanowire Growth.* Nano Lett., 2010. **10**(10): p. 4032-4039.
259. Mandl, B., et al., *Growth Mechanism of Self-Catalyzed Group III-V Nanowires.* Nano Lett., 2010. **10**(11): p. 4443-4449.
260. Sohn, J.I., et al., *Direct observation of the structural component of the metal-insulator phase transition and growth habits of epitaxially grown VO2 nanowires.* Nano Lett., 2007. **7**(6): p. 1570-1574.
261. San-Miguel, M.A., et al., *In situ growth of Ag nanoparticles on alpha-Ag2WO4 under electron irradiation: probing the physical principles.* Nanotechnology, 2016. **27**(22): p. 225703-225712.
262. Tsuji, M., et al., *Stepwise Growth of Decahedral and Icosahedral Silver Nanocrystals in DMF.* Cryst. Growth Des., 2010. **10**(1): p. 296-301.
263. Andres, J., et al., *Formation of Ag nanoparticles under electron beam irradiation: Atomistic origins from first-principles calculations.* Int. J. Quantum Chem., 2018. **118**(9).
264. Andrés, J., et al., *In situ Formation of Metal Nanoparticles through Electron Beam Irradiation: Modeling Real Materials from First-Principles Calculations.* J. Material Sci. Eng., 2018. **7**: p. 461.
265. Longo, E., et al., *In situ Transmission Electron Microscopy observation of Ag nanocrystal evolution by surfactant free electron-driven synthesis.* Sci. Rep., 2016. **6**: p. 21498.
266. da Silva, E.Z., et al., *Connecting Theory with Experiment to Understand the Sintering Processes of Ag Nanoparticles.* J. Phys. Chem. C, 2019. **123**(17): p. 11310-11318.
267. Faccin, G.M., et al., *Computational Modeling for the Ag Nanoparticle Coalescence Process: A Case of Surface Plasmon Resonance.* J. Phys. Chem. C, 2017. **121**(12): p. 7030-7036.
268. Sreedevi, A., et al., *Influence of electron beam irradiation on structural and optical properties of alpha-Ag2WO4 nanoparticles.* Micron, 2016. **88**: p. 1-6.
269. Roca, R.A., et al., *Formation of Ag nanoparticles on metastable beta-Ag2WO4 microcrystals induced by electron irradiation.* Chem. Phys. Lett., 2016. **644**: p. 68-72.

270. Machado, T.R., et al., *From Complex Inorganic Oxides to Ag–Bi Nanoalloy: Synthesis by Femtosecond Laser Irradiation.* ACS Omega, 2018. **3**(8): p. 9880-9887.
271. Añez, R., et al., *Unveiling the Ag-Bi miscibility at the atomic level: A theoretical insight.* Comput. Mater. Sci., 2021. **197**: p. 110612.
272. Cabral, L., et al., *Evidence for the formation of metallic In after laser irradiation of InP*. J. Appl. Phys., 2019. **126**(2).
273. Cabral, L., et al., *Formation of metallic Ag on AgBr by femtosecond laser irradiation.* Physchem., 2022. **Just Accepted**.
274. Assis, M., et al., *Unconventional Magnetization Generated from Electron Beam and Femtosecond Irradiation on α-Ag2WO4: A Quantum Chemical Investigation.* ACS Omega, 2020. **5**: p. 10052-10067.
275. Teixeira, M.M., et al., *α-Ag2WO4 under microwave, electron beam and femtosecond laser irradiations: Unveiling the relationship between morphology and photoluminescence emissions.* J. Alloys Compd., 2022. **903**: p. 163840.
276. Li, Q.Y., et al., *Facile fabrication and photocatalytic performance of WO3 nanoplates in situ decorated with Ag/beta-Ag2WO4 nanoparticles.* J. Environ. Chem. Eng., 2018. **6**(2): p. 1969-1978.

Journal Pre-proof

Figure Captions

Fig. 1. Schematic representation of the unit cell corresponding to **(a)** orthorhombic α-Ag_2WO_4, **(b)** hexagonal β-Ag_2WO_4, and **(c)** cubic γ-Ag_2WO_4. The cluster coordination numbers are highlighted.

Fig. 2. Schematic representation synthesis of α-$AgWO_4$ ceramics by the solid-state reaction method. **(a)** 1:1 stoichiometric mixture of the respective oxides (Ag_2O and WO_3), **(b)** several grinding cycles for oxides homogenization and surface contact improvement, **(c)** the final stage with calcination between (350—950 °C) at different times (2—24 h) of the homogenized oxides after several grinding cycles, respectively.

Fig. 3. Some procedures applied in the synthesis of the different polymorphs of Ag_2WO_4-based materials.

Fig. 4. A schematic representation of some available morphologies for α-Ag_2WO_4, β-Ag_2WO_4, and γ-Ag_2WO_4 polymorphs. The exposed surfaces at the morphology are highlighted.

Fig. 5. Various strategies used to improve the activity of Ag_2WO_4 polymorphs.

Fig. 6. α-Ag_2WO_4 structure with doping atoms at W and Ag sites.

Fig. 7. Schematic representation of the Ag_2WO_4 crystals grown on g-C_3N_4 sheet surfaces. The formation of g-C_3N_4/α-Ag_2WO_4 is energetically assisted by light, microwave (MW), and high temperature (T), while g-C_3N_4/β-Ag_2WO_4 is favored under room temperature (T).

Fig. 8. Schematic synthetic procedure for the obtention of Ag_2WO_4/AgX core-shell or heterostructure.

Journal Pre-proof

Fig. 9. Schematic representation of the VB, CB, and Fermi Level for the semiconductors (p- and n-type) and for the Ag_2WO_4 before and after the formation of the heterojunction.

Fig. 10. (a) Production of FE-SEM images from interacting electrons with α-Ag_2WO_4 structure, **(b)** Real-time FE-SEM images of Ag growth from α-Ag_2WO_4 structure: FE–SEM images taken with intervals of 2 min. FE–SEM of the same region where Ag filaments grow from the α-Ag_2WO_4 crystal surface. Ag filaments (blue arrows) grow while other Ag NPs are absorbed by the α-Ag_2WO_4 crystal surface (red arrows), indicating that there is a balance of clusters with the incidence of the EB, and (c) EDX image mapping Ag-L_3 from the α-Ag_2WO_4 crystal surface.

Fig. 11. Timeline showing some of the key milestones and advances in the field from 1973 until 2022.

Journal Pre-proof

Table

Table 1. The synthesis method, phase, and morphologies of Ag_2WO_4/oxide and Ag_2WO_4/metal-organic composites and their applications (RhB: Rhodamine B; TC-HCl: tetracycline hydrochloride; ThP: thiophene; MB: methylene blue; MO: methyl orange; VLI: visible-light irradiation).

Composite	Synthesis method	Phase	Morphology	Application	Ref.
Binary Oxides					
Ag_2WO_4/WO_3	Calcining method	α-Ag_2WO_4	Hierarchical flower-like hollow	RhB decolorization under VLI	[197]
Ag_2WO_4/c-ZnO	Hydrothermal	α-Ag_2WO_4	Nanorods with different average size distribution	Degrading the TC-HCl antibiotics	[199]
Ag/ZnO/Ag_2WO_4	Ultrasonic-irradiation	β-Ag_2WO_4	Micron Rods with different size	Photodegradation of RhB, MB, MO, and fuchsine under VLI	[200]
Mn_3O_4/ Ag_2WO_4	Microwave-assisted precipitation	α-Ag_2WO_4	Nanocomposites	Photooxidation of ThP under VLI	[201]
Ag/WO_3/ Ag_2WO_4	Simple precipitation	β-Ag_2WO_4	Ag/Ag_2WO_4 decorated on WO_3 nanoplates	Degradation of RhB, MB, and MO under VLI	[276]
Ternary Oxides					
$CaTiO_3/Ag_2WO_4$	Coprecipitation	α-Ag_2WO_4	Rod-shaped	Photoluminescence	[212]
$CaWO_4/Ag_2WO_4$	Hydrothermal	α-Ag_2WO_4	Rod-like	MB degradation under UV–VLI.	[213]
Ag_2WO_4/Ag_3PO_4	Chemical precipitation method	not detected (low concent.)	Regular NPs	Mineralization of Bisphenol A under simulated solar light irradiation	[214]
Ag/β-Ag_2WO_4 /$BiVO_4$	Hydrothermal and ultrasonic-	β-Ag_2WO_4	Spherically shaped	Selective oxidation of alcohols to	[215]

	irradiation			aldehydes.	
Ag_2WO_4/Ag /Bi_2MoO_6	Hydrothermal/ photochemical process	β-Ag_2WO_4	Ag_2WO_4/Ag NPs on Bi_2MoO_6 nanosheets surface	Degradation of MB under 410 nm LED	[216]
Ag_2WO_4 /$Bi_2Fe_4O_9$	Hydrothermal/ precipitation method	α-Ag_2WO_4	Ag_2WO_4 NPs on $Bi_2Fe_4O_9$ surface	RhB degradation under visible light	[217]
Ag_2WO_4 /Bi_2WO_6	Hydrothermal-precipitation	β-Ag_2WO_4	Ag_2WO_4 NPs on the Bi_2WO_6 nanosheets	Degradation of RhB	[227]
Metal-Organic Compounds					
Ti-based MOF (MIL-125-NH_2)	Simple *in-situ* precipitation	α-Ag_2WO_4	spherical Ag_2WO_4 NPs on micro MIL-125-NH_2.	MB and RhB photodegradation under UV and VLI.	[221]
Zr-based MOF (UiO-66)	Simple *in-situ* precipitation		Ag/Ag_2WO_4 on UiO-66 surface	Photodegradation of PBS (azo dye) and RhB under VLI	[222]
Co-phthalocyanine (CoPc)	Solvent evaporation	α-Ag_2WO_4	Irregular (rod/block like + spherical)		[223]
Fe-phthalocyanine (FePc)	Solvent evaporation	α-Ag_2WO_4	Irregular (rod/block like + spherical)		[103]

Journal Pre-proof

Figures:

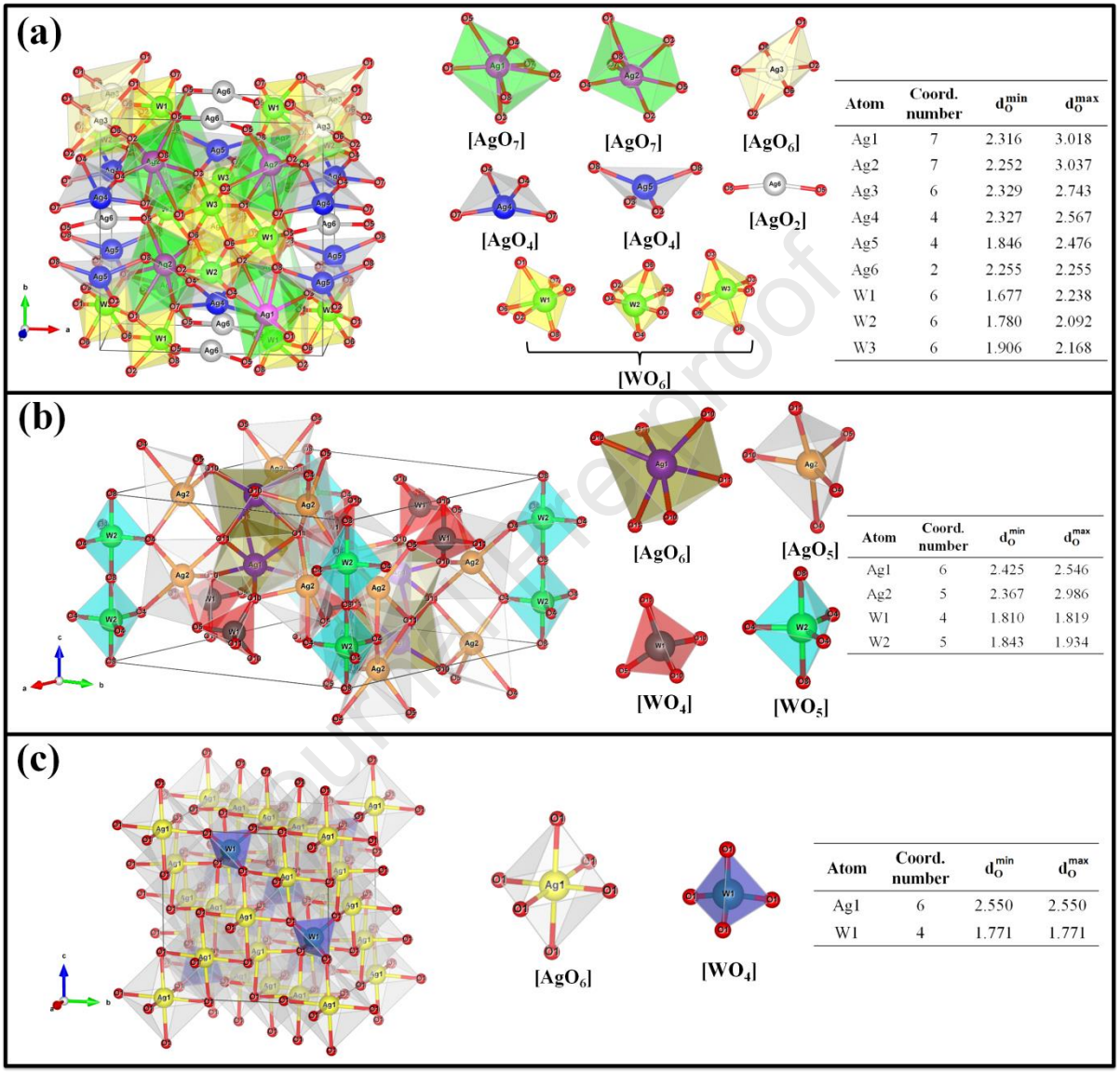

Atom	Coord. number	d_O^{min}	d_O^{max}
Ag1	7	2.316	3.018
Ag2	7	2.252	3.037
Ag3	6	2.329	2.743
Ag4	4	2.327	2.567
Ag5	4	1.846	2.476
Ag6	2	2.255	2.255
W1	6	1.677	2.238
W2	6	1.780	2.092
W3	6	1.906	2.168

Atom	Coord. number	d_O^{min}	d_O^{max}
Ag1	6	2.425	2.546
Ag2	5	2.367	2.986
W1	4	1.810	1.819
W2	5	1.843	1.934

Atom	Coord. number	d_O^{min}	d_O^{max}
Ag1	6	2.550	2.550
W1	4	1.771	1.771

<Figs. 1(a-c)>

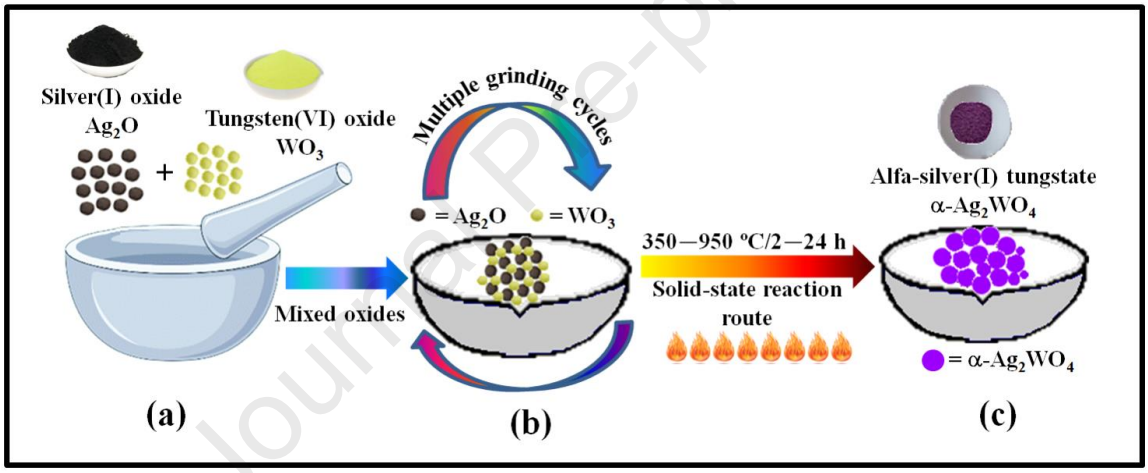
Silver(I) oxide
Ag_2O
Tungsten(VI) oxide
WO_3
Mixed oxides
Multiple grinding cycles
= Ag_2O
= WO_3
350—950 °C/2—24 h
Solid-state reaction route
Alfa-silver(I) tungstate
α-Ag_2WO_4
= α-Ag_2WO_4
(a)
(b)
(c)

<Fig. 2(a-c)>

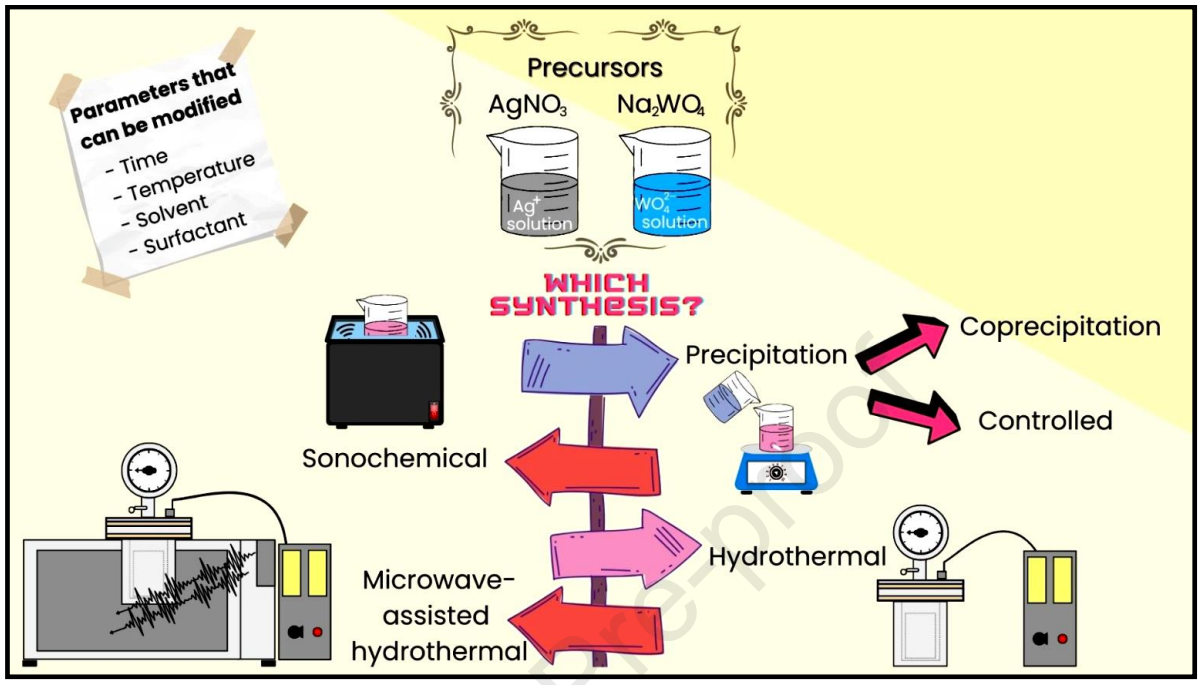

<Fig. 3>

Journal Pre-proof

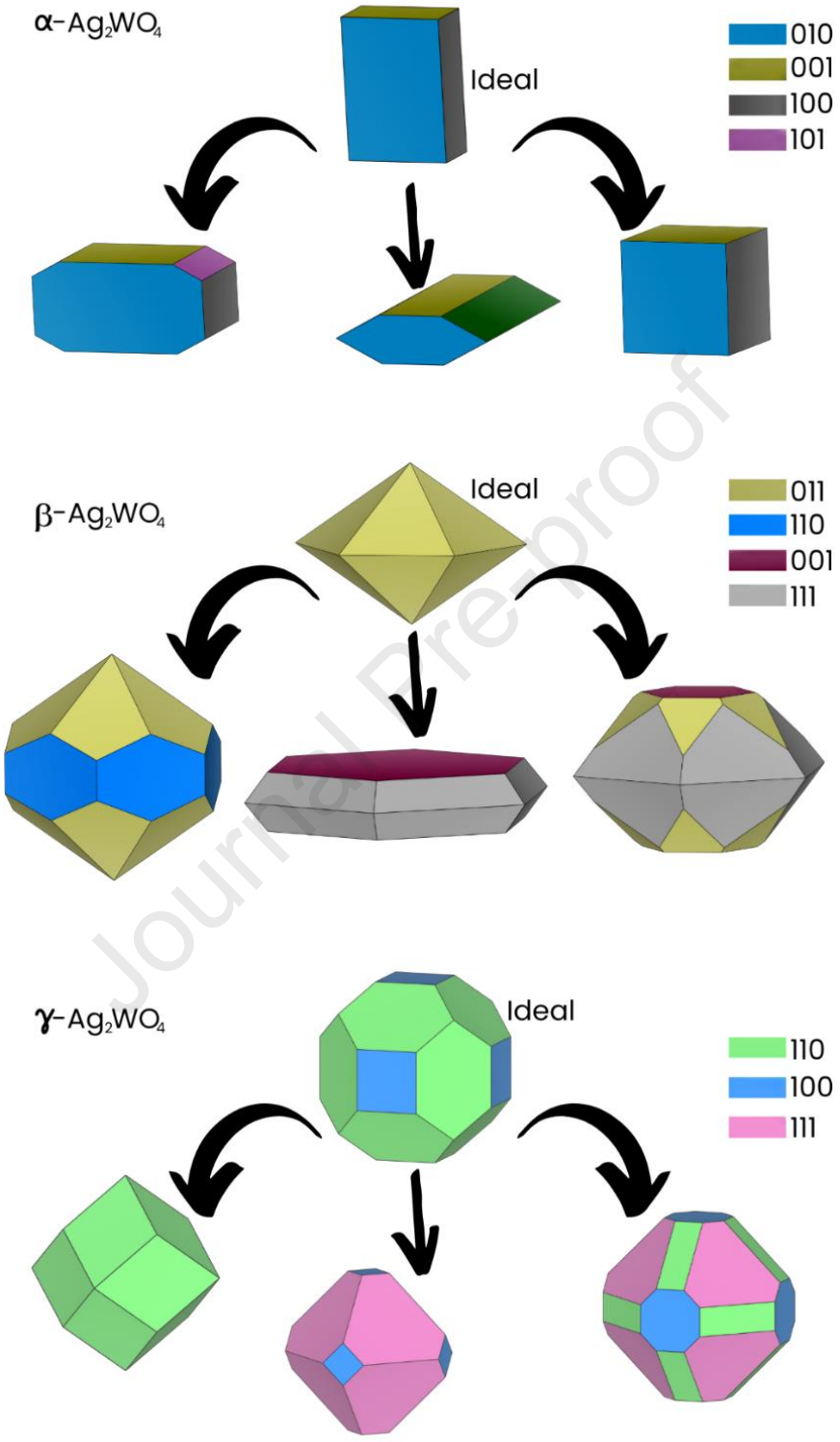

<Fig. 4>

Journal Pre-proof

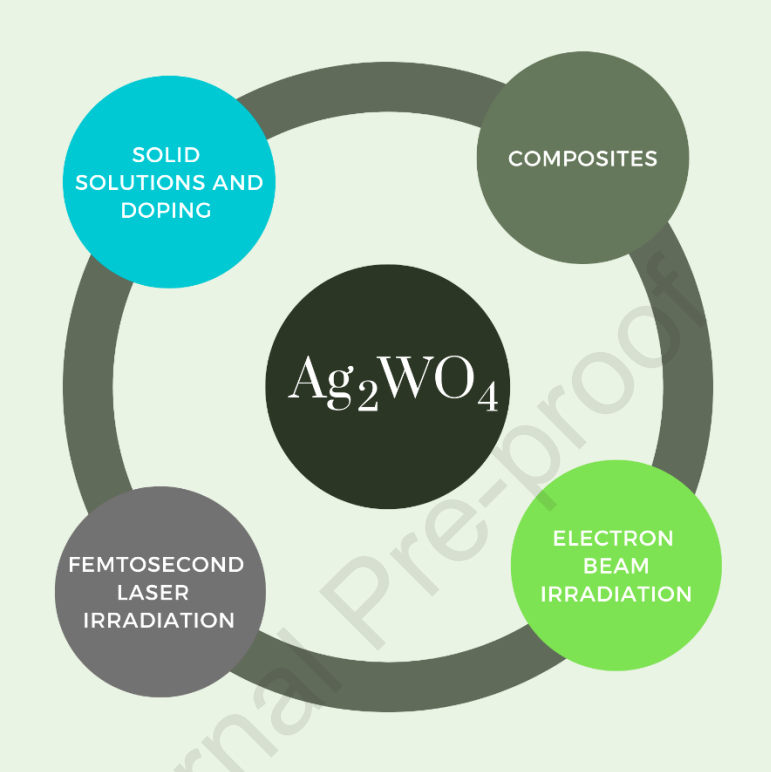

Journal Pre-proof

<Fig. 5>

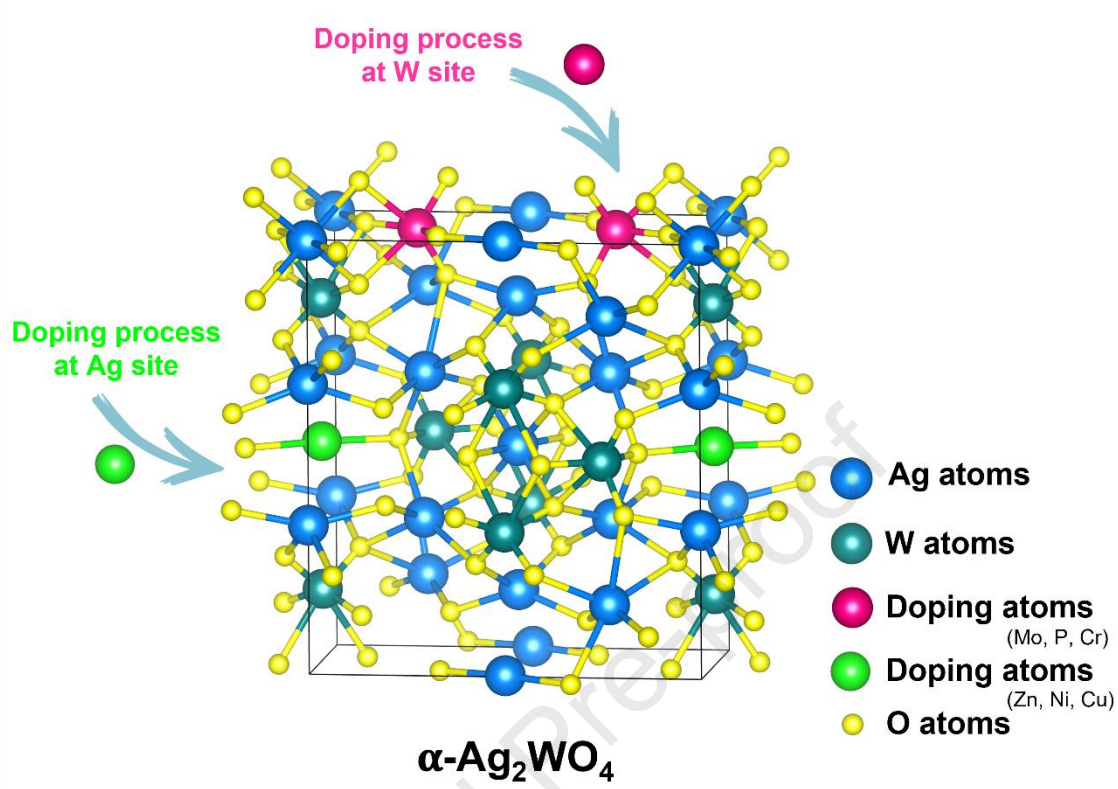

<Fig. 6>

Journal Pre-proof

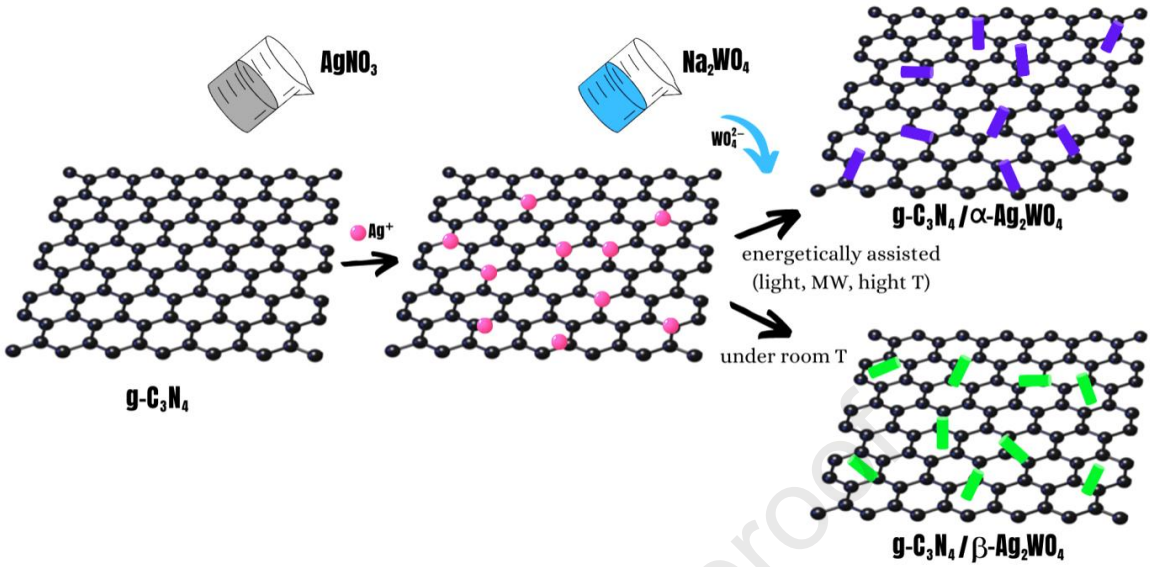

<Fig. 7>

Journal Pre-proof

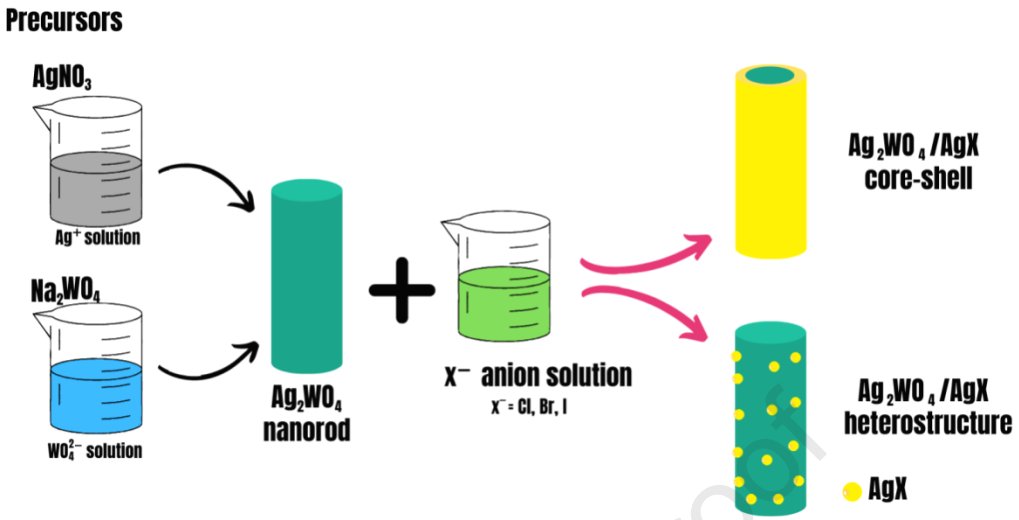

<Fig. 8>

Journal Pre-proof

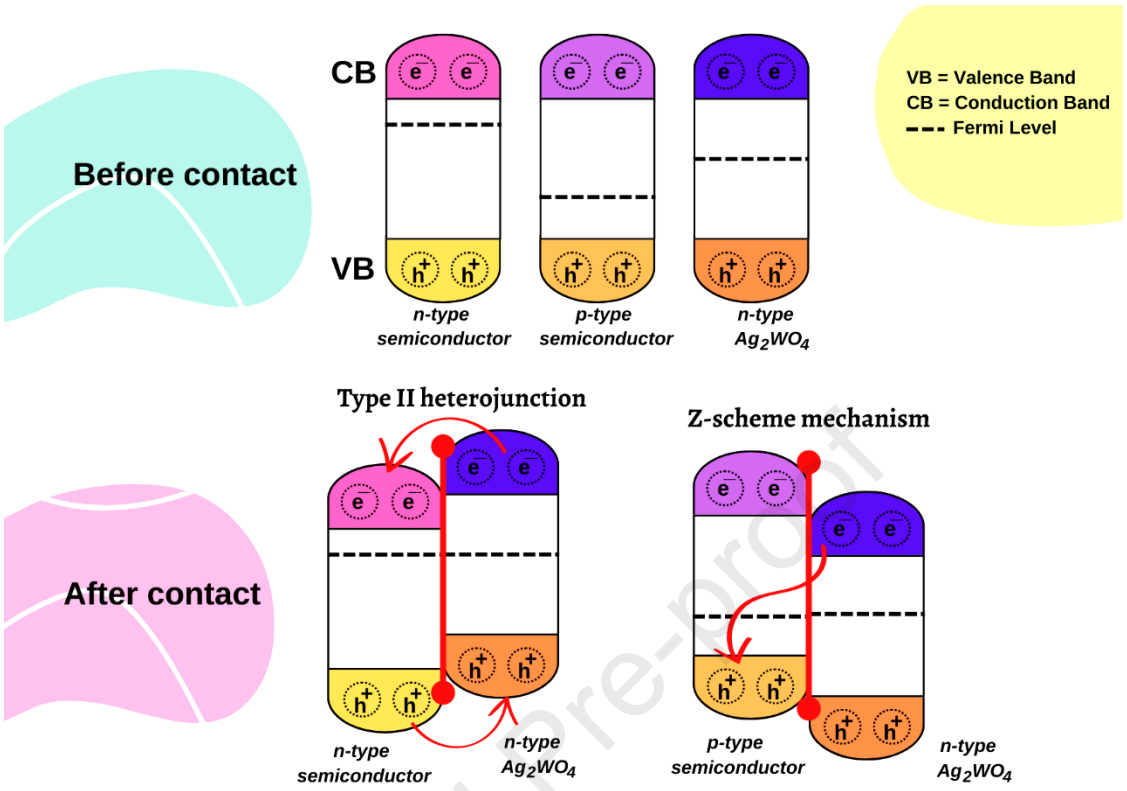

<Fig. 9>

Journal Pre-proof

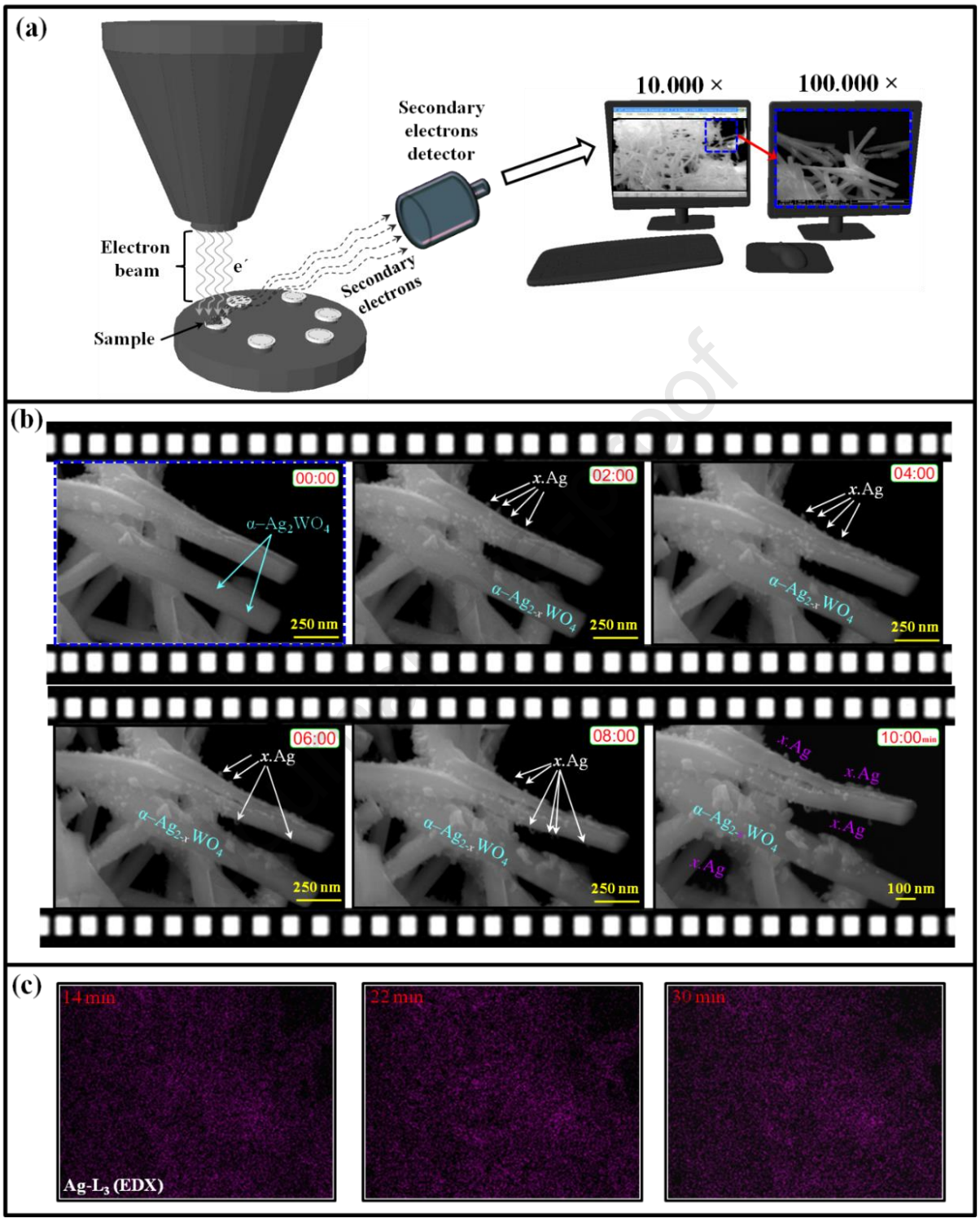
(a)
Secondary electrons detector
10.000 ×
100.000 ×
Electron beam
e´
Secondary electrons
Sample
(b)
00:00
α–Ag2WO4
250 nm
02:00
x.Ag
α–Ag2-x WO4
250 nm
04:00
x.Ag
α–Ag2-x WO4
250 nm
06:00
x.Ag
α–Ag2-x WO4
250 nm
08:00
x.Ag
α–Ag2-x WO4
250 nm
10:00min
x.Ag
α–Ag2-x WO4
100 nm
(c)
14 min
22 min
30 min
Ag-L3 (EDX)

<Figs. 10(a–c)>

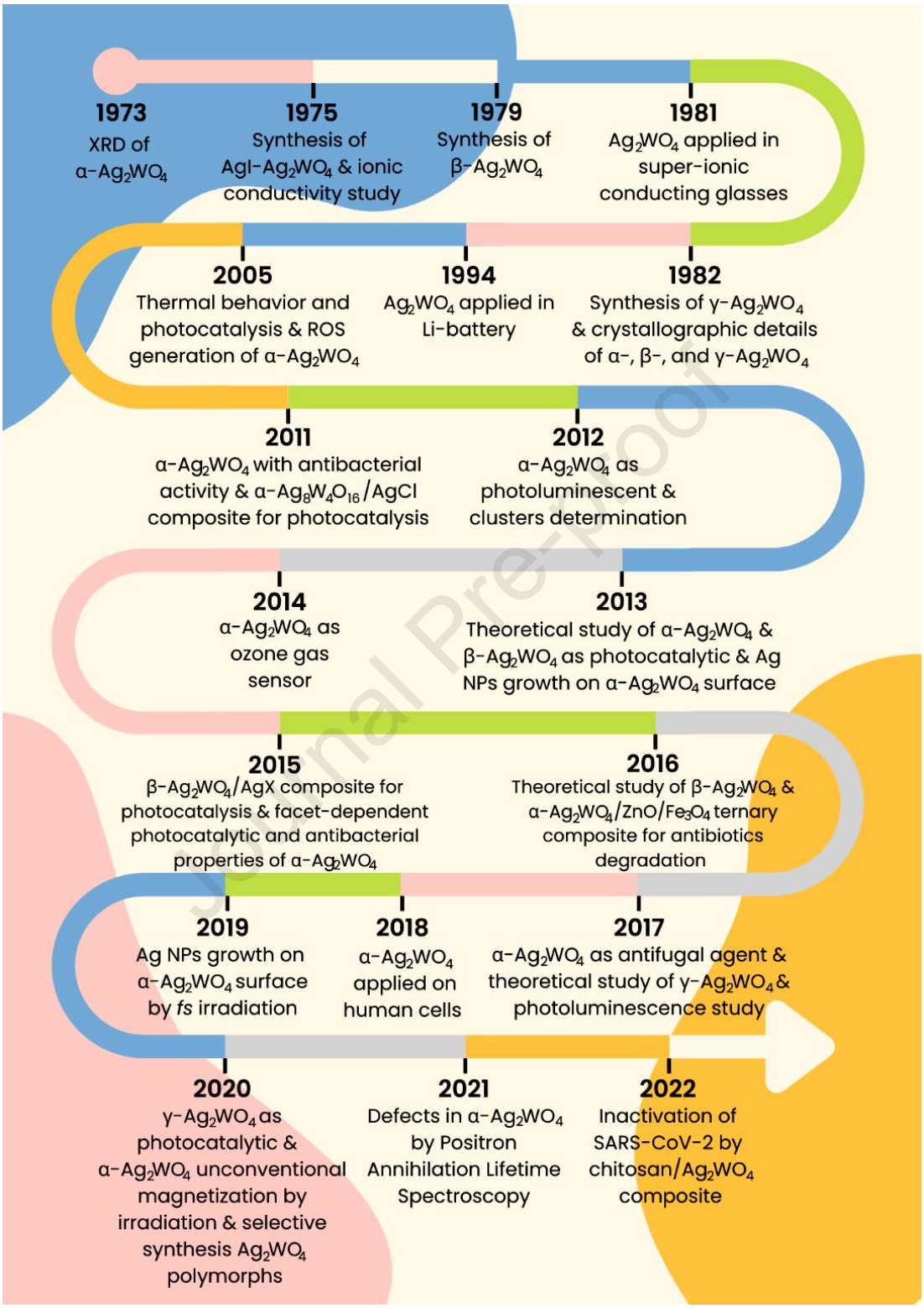
1973
XRD of α-Ag_2WO_4
1975
Synthesis of AgI-Ag_2WO_4 & ionic conductivity study
1979
Synthesis of β-Ag_2WO_4
1981
Ag_2WO_4 applied in super-ionic conducting glasses
2005
Thermal behavior and photocatalysis & ROS generation of α-Ag_2WO_4
1994
Ag_2WO_4 applied in Li-battery
1982
Synthesis of γ-Ag_2WO_4 & crystallographic details of α-, β-, and γ-Ag_2WO_4
2011
α-Ag_2WO_4 with antibacterial activity & α-$Ag_8W_4O_{16}$/AgCl composite for photocatalysis
2012
α-Ag_2WO_4 as photoluminescent & clusters determination
2014
α-Ag_2WO_4 as ozone gas sensor
2013
Theoretical study of α-Ag_2WO_4 & β-Ag_2WO_4 as photocatalytic & Ag NPs growth on α-Ag_2WO_4 surface
2015
β-Ag_2WO_4/AgX composite for photocatalysis & facet-dependent photocatalytic and antibacterial properties of α-Ag_2WO_4
2016
Theoretical study of β-Ag_2WO_4 & α-Ag_2WO_4/ZnO/Fe_3O_4 ternary composite for antibiotics degradation
2019
Ag NPs growth on α-Ag_2WO_4 surface by *fs* irradiation
2018
α-Ag_2WO_4 applied on human cells
2017
α-Ag_2WO_4 as antifugal agent & theoretical study of γ-Ag_2WO_4 & photoluminescence study
2020
γ-Ag_2WO_4 as photocatalytic & α-Ag_2WO_4 unconventional magnetization by irradiation & selective synthesis Ag_2WO_4 polymorphs
2021
Defects in α-Ag_2WO_4 by Positron Annihilation Lifetime Spectroscopy
2022
Inactivation of SARS-CoV-2 by chitosan/Ag_2WO_4 composite

<Figs. 11>

Highlights

- Synthesis of Ag_2WO_4 polymorphs and their structures.
- Multifunctional properties of Ag_2WO_4-based materials.
- Improving the property and functionality of Ag_2WO_4-based materials.
- A timeline of the key milestones.

Journal Pre-proof

Journal Pre-proof

Author Biography

AMANDA FERNANDES GOUVEIA is post-doc research at the Laboratory of Theoretical and Computational Chemistry in the Jaume I University, Castellon (Spain). Her Ph.D. was completed at the Federal University of São Carlos (Brazil). She did a post-doctorate at the State University of Piauí and at the State University of Campinas and received the Nano-Micro Science Innovation Award at the Nano-Micro Conference (South Korea, 2018). She works in the interdisciplinary areas from Chemistry, Inorganic Chemistry, Physical Chemistry, Materials Chemistry, to Nanotechnology. Her original approach is based on coupling theory and simulation to experimentation in the following topics: semiconductors, photocatalytic and biocide activity.

ROMAN ALVAREZ ROCA received his BS and MS degrees in Physics from Havana University in 1994 and 2001, respectively, and his PhD degree in Materials Science and Engineering from Federal University of São Carlos in 2013. From

1994 to 2008, he worked as full-time professor in the Physics Department at Oriente University. From 2013 to present, works as research fellow in the Chemistry Department at Federal University of São Carlos. His held several post-doctoral, at current has stay as post-doc research at Postgraduate Program of Chemistry at Federal Institute of Maranhao. The research interest focuses on the synthesis, processing, and properties of novel functional nanostructured materials for photocatalytic applications. More information can be found on: http://lattes.cnpq.br/8280667063040918.

NADIA GUERRA MACEDO is currently a post-doc researcher at the Group of Photoelectrochemistry & Energy Conversion at the State University of Campinas (Brazil). Her Ph.D. was completed at the University of Sao Paulo (Brazil). AFG did a first post-doctorate at the Federal University of São Carlos (Brazil). She works in interdisciplinary areas like Inorganic Chemistry, Physical Chemistry, Materials Chemistry and Nanotechnology. She has experience with carbon-based nanomaterials, micro-nano composites, semiconductors, photocatalysts and her current interests are in the field of photoelectrochemistry.

Journal Pre-proof

LAÉCIO SANTOS CAVALCANTE is Adjunct II Professor at the Universidade Estadual do Piauí-UESPI-CCN-DQ, CNPq-PQ-2 productivity scholarship, and carrying out their research in the GERATEC-CETEM- GrEEnTec laboratories since 2013 at Brazil-Teresina-PI. He has published 7 book chapters, as well as around 150 scientific papers most of them in top-level international journals in themes related to semiconductor materials (synthesis Methods; structural characterization; cluster coordination; photoluminescence; photocatalysis, colorimetry, sensors, bactericide, supercapacitores, and catalysts). Currently has an index-H: 53 (Scopus).

ELSON LONGO is Professor Emeritus of the Department of Chemistry at UFSCar, professor HONORIS CAUSA at UFPB. Doctor in Physical Chemistry from USP, he has published more than 1,363 articles in international journals, H Index 83, 35,747 citations. He supervised and co-supervised more than 170 theses and dissertations. He has received over 23 awards and honorable mentions. Director of the Center for the Development of Functional Materials (CDMF/FAPESP). Member of the World Academy of

Journal Pre-proof

Ceramics, Academy of Sciences of the State of São Paulo (ACIESP) and the Brazilian Academy of Sciences (ABC).

MIGUEL ANGEL SAN-MIGUEL is currently an Associate Professor in Physical Chemistry at the State University of Campinas (Brazil) since 2014 and leads the Unicamp Materials Simulation Lab (UMSL). He completed his Ph.D. in 1998 at the Universidad de Sevilla (Spain), where worked as an Associate Professor in Physical Chemistry until 2014. He held several post-doctoral stays at the Universities of Reading and Warwick (UK) and as Visiting Professor at the University of Oxford (UK). He works in atomistic modeling using both classical and quantum methods in Materials Science. His main research interests include chemical reactivity, biomaterials, and heterogeneous catalysis.

ANGELA ALTOMARE is Research Director at the Institute of Crystallography of National Research Council of Italy in Bari. Her research

activity is mainly devoted to the development and application of innovative crystallographic methodologies for structural characterization of crystalline compounds, inorganic, organic and metalorganic, from single crystal and microcrystalline powder diffraction data. She has published around 150 papers in indexed international journals and 10 chapters of books (two chapters in the 'International Tables for Crystallography, Volume H'). She is co-author of twelve crystallographic computing programs worldwide used. Her scientific competence is widely recognized by the community at national and international levels, as proved by the number of citations greater than 30000 (Google Scholar, June 2022).

GILMAR SILVÉRIO DA SILVA area of scientific activities is analytical chemistry, environmental chemistry and materials. He did the post-doctoral at the Aveiro University, Portugal and the Doctoral at the Campinas University (UNICAMP). He is a full professor at the Department of Chemistry at the Federal Institute of Maranhão (IFMA) and permanent member of the master and doctoral programs in chemistry.

Journal Pre-proof

JUAN ANDRES is Full Professor of Physical Chemistry and director of the Laboratory of Theoretical and Computational Chemistry at Jaume I University, Castellon (Spain). In 2000, this Laboratory reached the consideration of Center of Excellence Marie-Curie from European Union and has been established in a broad sphere of action in which chemistry, physics, quantum mechanics, materials and surfaces science, catalysis and nanotechnology converge. He has published 20 book chapters, as well as around 500 scientific papers, most of them in top-level international journals in this interdisciplinary fields.

Journal Pre-proof

Journal Pre-proof

Declaration of interests

☒ The authors declare that they have no known competing financial interests or personal relationships that could have appeared to influence the work reported in this paper.

☐ The authors declare the following financial interests/personal relationships which may be considered as potential competing interests:

Journal Pre-proof